A Study of Charge Probe Response on a Junction
of Unequal Radii Thin Wires

Santiago Singarayar
B. M. Duff
University of Mississippi

Abstract

The experimental measurement of charge density induced on conducting

surfaces often makes use of a short monopole as the charge probe. Measure-

ments on structures containing junctions of unequal radii cylinders have

been hampered by incomplete knowledge of the probe characteristics. An

investigation of charge probe response as related to the radius of the

cylinder on which it is mounted is reported here. An experimental determin-

ation of the ratio of probe response when mounted on two different radii

cylinders has been conducted using a coaxial line geometry with a step

change in radius of the inner conductor. In addition, a theoretical solution

in numerical computations of the probe response in relation to the radius of

the cylinder upon which it is mounted has been conducted. The results of

these studies are presented in the following report.

TABLE OF CONTENTS   Page

LIST OF FIGURES

Chapter I

INTRODUCTION

The measurement of the current and charge distributions on antennas and scatterers is important in order to gain an understanding of their electromagnetic behavior and to aid in developing and checking of theoretical solutions. The basic techniques for making these measurements have been established for some time and used by many investigators. However, during a recent experimental project, to be described below it became obvious that more accurate knowledge of the response characteristics of charge probes was necessary. The resulting investigation of charge probe response forms the basis of this thesis.

The experimental project which leads to the investigation reported here, concerned the measurement of charge distribution induced on structures containing junction of thin wires of unequal radii. The purpose of that investigation was to experimentally determine the appropriate condition on charge which should be applied in theoretical solution of this type of structure.

A theoretical analysis and discussion of the junction has been presented by T.T. Wu and R.W.P. King [3]. The probe used for the measurement of charge distribution consisted of a very short monopole mounted on the surface of the cylindrical structure. For the experimental determination of the charge condition at the

junction, an accurate knowledge of the probe response as a function of the radius of the cylinder upon which it is mounted is necessary. A charge probe mounted on a cylindrical structure has been analysed theoretically by R.W.P. King [1] and experimentally by Whiteside [2]. However, these investigations do not provide sufficiently accurate solutions for the probe response as a function of the radius of the cylindrical structures. An independent experimental and theoretical investigation of the charge probe response has been conducted, the results of which are presented in this thesis.

Chapter II deals with the measurement technique by which the probe calibration factor can be determined. This probe calibration factor has been determined for 3 different probe heights for 2 junctions of thin wires of 5/16" to 1/8" radii and 3/16" to 1/8" radii. To make sure that the probe calibration factor is the same for all charge conditions at the junction, the probe calibration factor has been determined for 3 different charge conditions namely maximum, minimum, and a condition in between maximum and minimum. The experimental data was analysed by using modified Prony's method.

A numerical solution for the current induced in the probe has been carried out using moment method techniques [4,5]. The analysis models the probe as a monopole receiving antenna perpendicular to an infinite plane conductor, but includes the incident $\bar{E}$ field variation which is to be expected when the probe is mounted on a cylinder. Chapter III deals with the methods used for this numerical analysis.

Finally, in Chapter IV, the experimental data, the results and
the conclusion are presented.

CHAPTER II

MEASUREMENT TECHNIQUE

(i) Introduction

The measurement of the surface charge density on a conductor may
be related to a measurement of $\bar{E}$ field by using the boundary condition,

$$\hat{n} \cdot \varepsilon_0 \bar{E} = \eta \qquad\qquad (2.1)$$

where ε_0 is the relative permittivity, $\hat{n}$ is the unit normal vector to
the surface of the test structure under consideration and η is the
surface charge density. It is therefore possible to obtain the surface
charge density by using a sensor whose output is proportional to the
normal component of the $\bar{E}$ field at the surface. The most common method
uses a short monopole receiving antenna, as shown in Fig. (2.1), which
is perpendicular to the surface of the test structure. The signal
induced in the load is however related to the $\bar{E}$ field along the entire
length of this monopole rather than simply the field at the surface.
If the normal component of the $\bar{E}$ field is constant over the length of
the probe there is no problem. But generally this is not the case.
In order to relate the monopole probe response to the charge density
on the test structure it is therefore necessary to have some knowledge
of the manner in which $\bar{E}$ varies over a short distance away from the
surface.

charge probe

Locking pin

Probe tube

Semi rigid
Coaxial cable
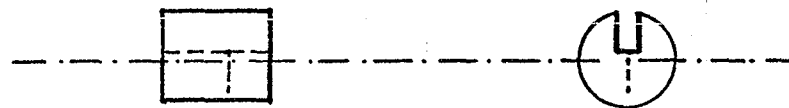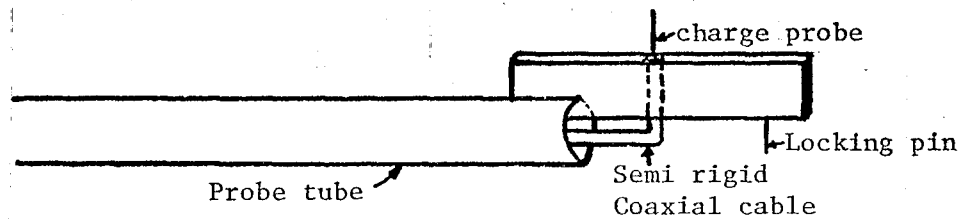
(a) Probe carriage for smaller radius tube.
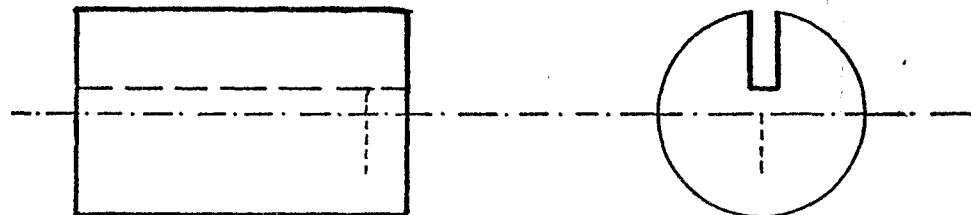
(b) Probe carriage for larger radius tube.

Fig. (2.1) CHARGE PROBE.

The present work considers only test structures composed of electrically thin conducting cylinders. The field produced by a uniformly charged infinite cylinder is known to vary as $\frac{1}{\rho}$. If the test structure (a cylindrical antenna) is of electrically thin radius and the probe is electrically short, then $\bar{E}$ over the length of the probe is controlled primarily by the local charge distribution. The field then becomes essentially the same as that of an infinite cylinder and $\bar{E}$ is very nearly proportional to $\frac{1}{\rho}$. This assumption is not valid near discontinuities of the conducting surface, however. The effect of this variation on the response of the probe depends on the radius of the test structure. To illustrate this effect, Fig. (2.2) presents $\frac{1}{\rho}$ plotted as a function of $(\rho-a)$ for three different cylinder radii. For a given probe height, the variation of E_ρ over the length of the probe is less when the probe is mounted on a large radius cylinder.

The effect of the $\frac{1}{\rho}$ variation may be reduced by reducing the probe height. However, the signal induced across the load is also reduced and so the signal to noise ratio. A second effect of changing the radius of the test structure is that the image plane for the monopole probe is of different radius of curvature. The fact that the charge probe is of finite size and it responds to fields away from the surface of the test structure makes it necessary to determine a probe calibration factor as a function of cylinder radius in an exact manner.

To determine the probe calibration factor experimentally, a system containing cylinders of different radii and for which the variation of the charge density as a function of cylinder radius can be predicted

10

$\dfrac{1}{(\rho)}$

$(\rho-a)$ in inches.
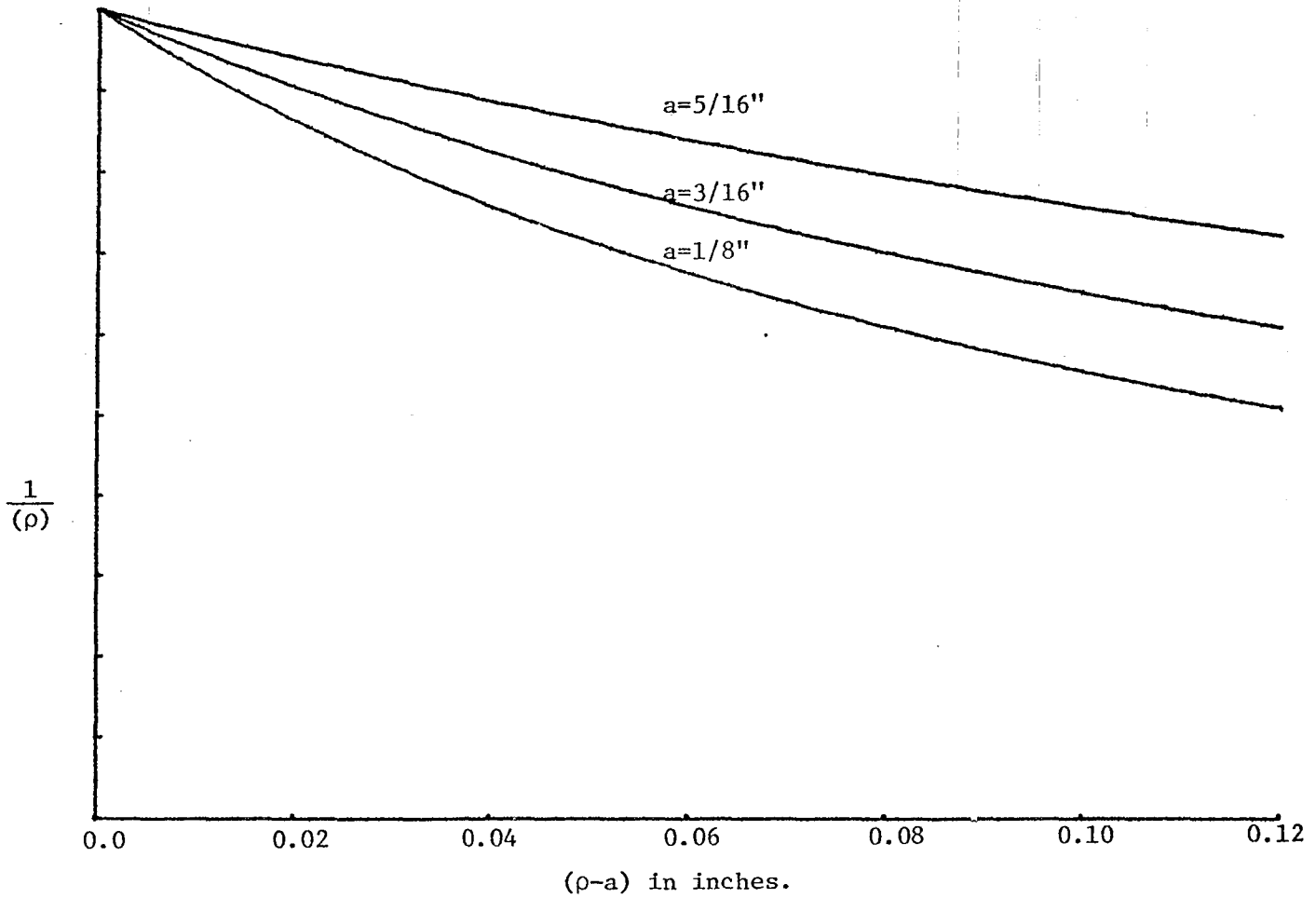
Fig. (2.2) $\dfrac{1}{\rho}$ VARIATION AS A FUNCTION OF $(\rho-a)$.

a=5/16"

a=3/16"

a=1/8"

11

is needed. The system chosen was a coaxial line with step change in the radius of the inner conductor. This system is shown in Fig. (2.3) and has been analysed by Marcuvitz[6]. The TEM mode $\bar{E}$ field distribution of the above system is shown in Fig. (2.4). The $\bar{E}$ field is uniform and proportional to $\frac{1}{\rho}$ inside the coaxial line except near the junction. The local effect near the junction can be replaced by a shunt capacitance so that the Kirchoff's current law is satisfied. At the junction the voltage is continuous making it easy to analyse the charge condition at the step in the following way.

(ii) Analysis of Coaxial Transmission Line

Fig. (2.5) illustrates a coaxial transmission line with a TEM mode propagation. In cylindrical coordinates the two dimensional Laplace equation is,

$$\frac{1}{\rho} \frac{\partial}{\partial \rho} (\rho \frac{\partial \Phi}{\partial \rho}) + \frac{1}{\rho^2} \frac{\partial^2 \Phi}{\partial \phi^2} = 0 \qquad (2.2)$$

For a potential function independent of angular coordinate ϕ, eq. (2.2) reduces to

$$\frac{1}{\rho} \frac{\partial}{\partial \rho} (\rho \frac{\partial \Phi}{\partial \rho}) = 0 \qquad (2.3)$$

The solution of equation (2.3) may be expressed as,

$$\Phi = c_1 \ln(\rho) + c_2 \qquad (2.4)$$

Imposing the boundary conditions $\Phi = V_0$ at $\rho = a$ and $\Phi = 0$ at $\rho = b$, eq. (2.3) yields the final solution for the potential as,

12

Charge Probe

Movable Short

ρ

z

a_2

a_1

b

Step radius system
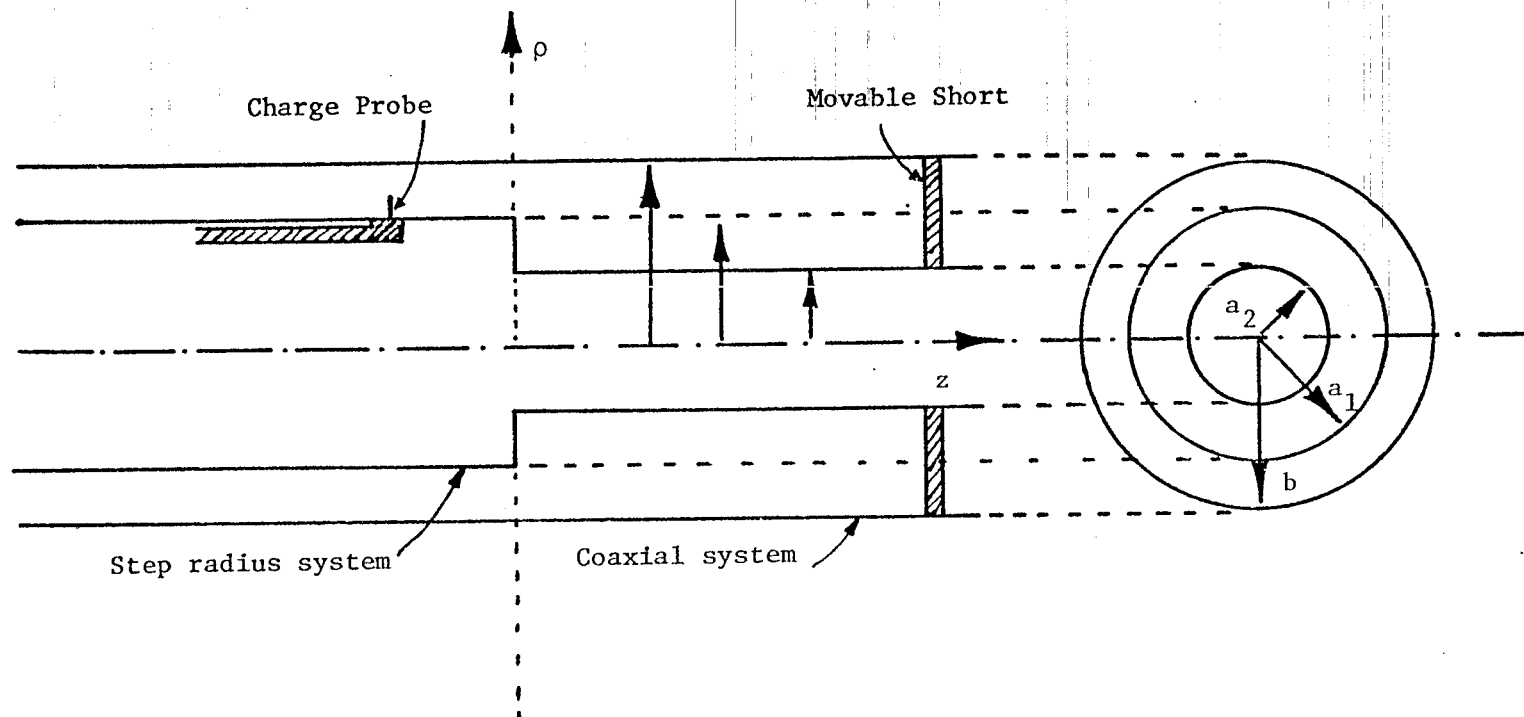
Coaxial system

Fig. (2.3)   COAXIAL SYSTEM WITH STEP RADIUS SYSTEM.
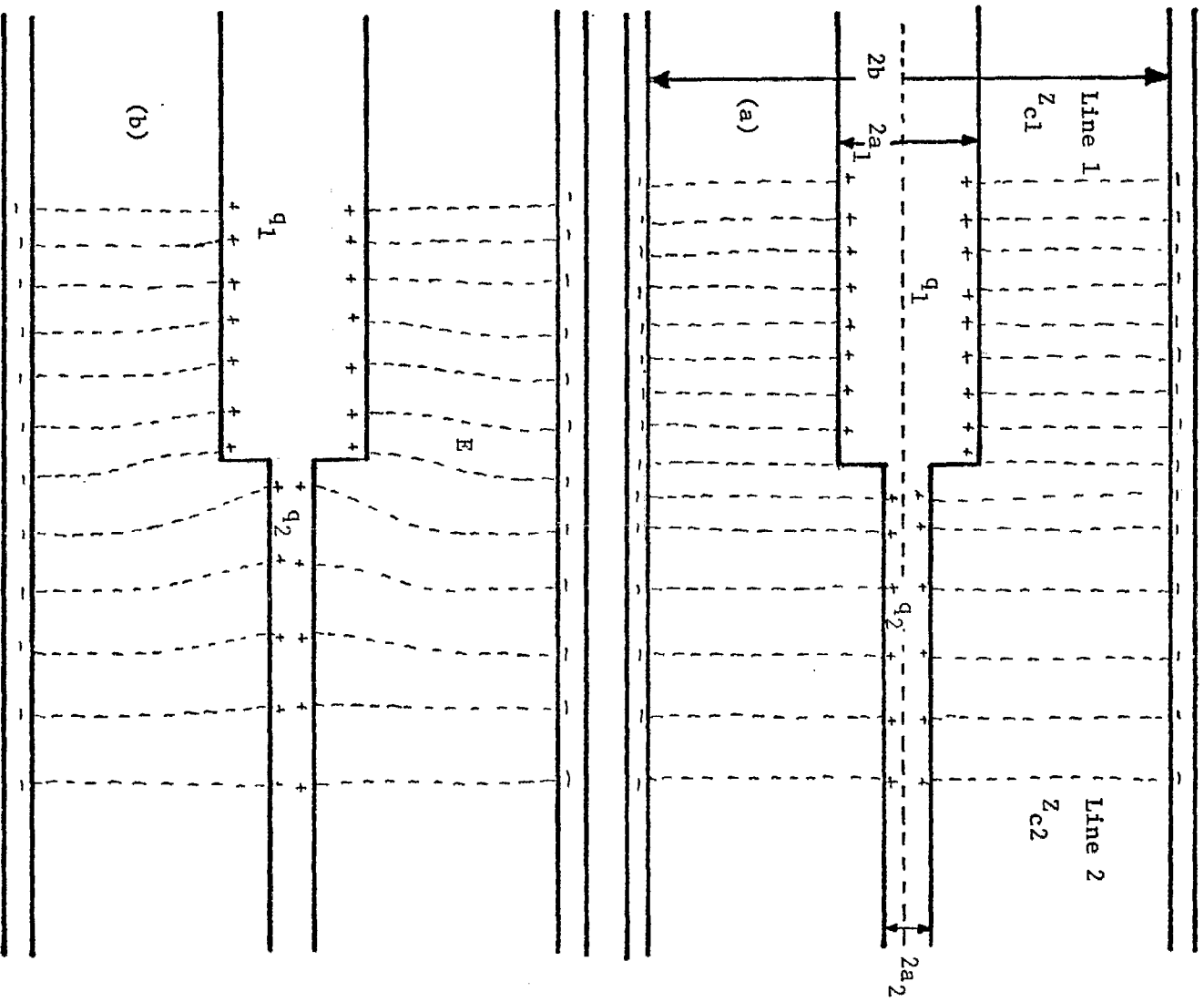
Fig. (2.4) (a) Zero order (b) Approximate Actual Distributions
of Charge per unit length and Radial E field in Coaxial
Line.

14

b

a_1

ρ

ϕ

$\Phi = V_0$

_____ $\bar{E}$ field

__ __ __ $\bar{H}$ field
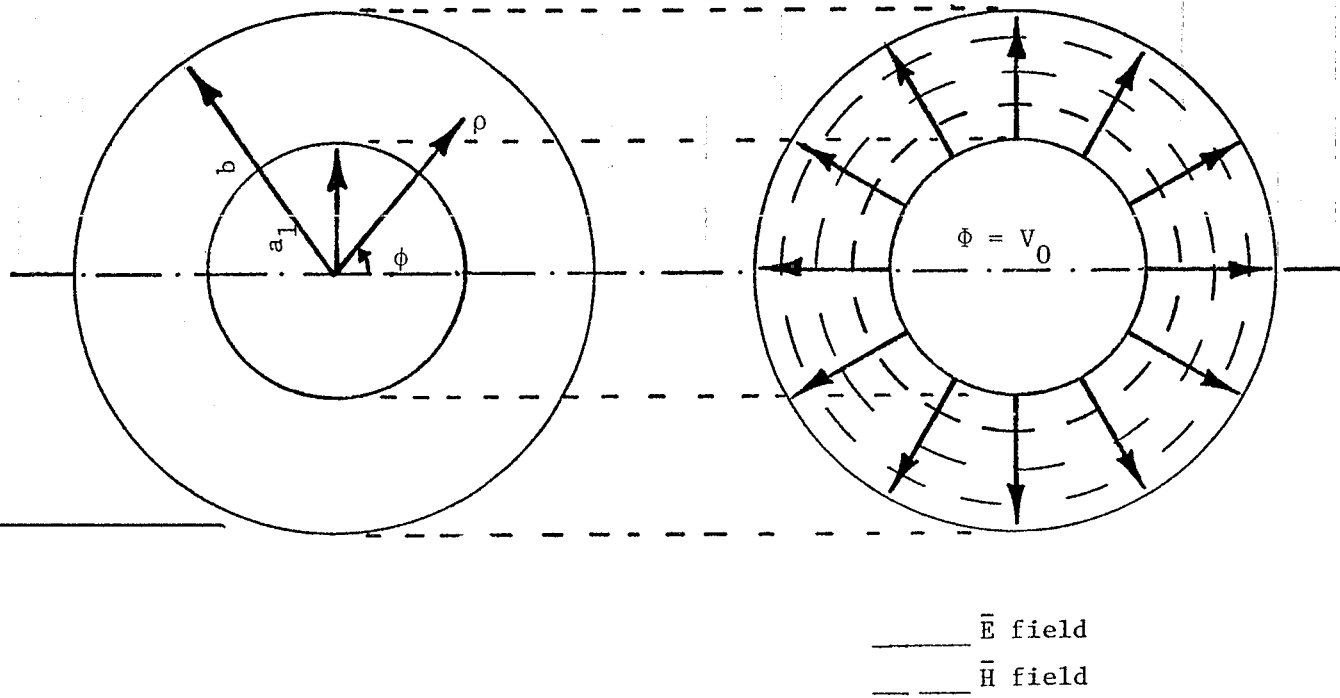
Fig. (2.5) Coaxial transmission line.

an associated charge density which differs from that of a TEM mode as indicated in Fig. (2.4)(b).

The voltage is continuous at the junction but because of the different radii, a difference in the magnitude of charge density exists at the junction. The ratios of linear and surface charge densities at the junction are given by

$$\frac{q_1}{q_2} = \frac{C_1 V_0}{C_2 V_0} = \frac{\ln\left(\frac{b}{a_2}\right)}{\ln\left(\frac{b}{a_1}\right)} \qquad (2.9)(a)$$

$$\frac{\eta_1}{\eta_2} = \frac{a_2}{a_1} \frac{\ln\left(\frac{b}{a_2}\right)}{\ln\left(\frac{b}{a_1}\right)} \qquad (2.9)(b)$$

(iii) Description of the Measurement System

A block diagram of the measurement system is given in Fig. (2.6). The commercial instruments used in the system are given in the block diagram itself.

The power at 300 MHz is fed to the amplifier. The amplifier signal is fed to the coaxial system through a balanced feed to avoid higher order mode propagation. Matching of the amplifier output to the coaxial system is done through a single stub tuner. The reference signal to the vector voltmeter reference channel is taken from the amplifier output with proper attenuation. The signal to the frequency meter is also is taken from the amplifier output with proper attenuation. The signal from the charge probe is fed to the test channel

$$\Phi = V_0 \ln\left(\frac{\rho}{b}\right) / \ln\left(\frac{a_1}{b}\right) \qquad (2.5)$$

$\bar{E}$ field of TEM mode in +z direction,

$$\bar{E} = - \nabla_t \Phi \, e^{-jkz} \qquad (2.6)$$

where k is the propagation constant.

Using eq. (2.5) $\bar{E}$ may be expressed as,

$$\bar{E} = \frac{V_0}{\ln\left(\frac{b}{a_1}\right)} \frac{\hat{a}_\rho}{\rho} \, e^{-jkz} \qquad (2.7)$$

The surface density of charge η_1 on an inner conductor of radius a_1, at z=0 may be obtained from eq. (2.7) and the boundary condition eq. (2.1) as,

$$\eta_1 = \frac{\varepsilon_0}{a_1 \ln\left(\frac{b}{a_1}\right)} \cdot V_0 \qquad (2.8)$$

Equation (2.8) can be written as,

$$q_1 = C_1 \, V_0$$

where C_1 is the capacitance per unit length and $q_1 = 2\pi a_1 \eta_1$ is the linear charge density. The same relationship applies to the inner conductor of radius a_2.

It must be remembered that the above analysis assumes that only TEM mode fields exist and that the junction is represented by a lumped shunt capacitance. The effect of the step change of radius is actually distributed over some short distance on either side of the junction with

17

of the vector voltmeter. The power level is monitored by the broad-band sampling meter to compensate for the drift in power level.

The magnitude or the phase of the signal is switched to the digital voltmeter by means of the relay actuator. The calculator samples this output 5 to 10 times and takes the average to minimize the effect of the minute fluctuations in the probe signal. The magnitude and phase quantities are stored in the calculator for later plotting and for further use.

The stepped radius coaxial line was constructed from cylindrical brass tubing. The three different inner conductor radii 0.3125" (0.79375 cm), 0.1875"(0.47625 cm), and 0.125"(0.3175 cm) were selected as being available readily. Two inner conductor systems were constructed one composed of 0.3125" and 0.125" radius tubing, the other of 0.1875" and 0.125" radius tubing. A tube of 1.0" inside diameter was used as the outer conductor. The space between inner and outer conductor was filled with styrofoam. A slot of 1/19"(0.13368 cm) was cut axially in the inner conductor tubing to allow movement of the charge probe along the structure. The probe carriage was designed to slide inside of the inner conductor tube and extend through the slot to the surface of the tube so that the structure is electrically continuous. The charge probe was constructed on a probe carriage using a semi rigid coaxial cable. The charge measurement was con-ducted on two different radii tubes. If two different probes had been used it would have been necessary that they be constructed identically.

Otherwise, it would have become necessary to calibrate them independently. To avoid this problem, a single charge probe with two different probe carriages was used. The wall thickness of the tubes had to be taken into consideration while making the probe carriage. For example for the 0.3125" radius tube wall thickness was 0.06"(0.1524 cm) and the 0.125" radius tube was 0.04". The probe carriage fit exactly inside of the tube and through the slot to the surface so that the charge probe was effectively mounted on the surface of the inner conductor tube. The cable used for making the probe was UT 20 manufactured by Uniform Tubes, Inc., with the following specifications.

Impedance: 50 Ohms

Outside diameter: 0.023"(0.05842 cm)

Center conductor diameter: 0.0045"(0.01143 cm)

The outer conductor of the cable was soldered to the probe carriage and cut at the surface. The dielectric insulator on the inner conductor was removed so that the inner conductor extended beyond the surface to form the monopole antenna. It was necessary that this monopole be straight and perpendicular to the test structure. The signal from the probe was carried by a coaxial cable contained inside of the inner conductor tube. Care was taken to see that stray pickup did not affect the signal by shielding the signal cables. A 1/8" diameter tube attached to the probe carriage was used both to protect the signal cable and to provide a means of positioning the probe.

The charge density measurement was made at intervals of 1 cm. The actual $\bar{E}$ field distribution near the step due to local effect made the measured result unreliable in this region. Moreover the charge probe was mounted at the center of the probe carriage which made it impossible to reach the step in the large radius tube. For analysis of the data, a few data points were eliminated near the junction to eliminate the local effect and the data was analysed by using a modofied Prony's method to fit curves to the TEM mode distribution. This procedure will be discussed separately.

Measurements were made for probe heights of 0.10"(0.2540 cm) to 0.06"(0.1524 cm) at an interval of 0.02"(0.0508 cm). The charge condition at the junction was varied by using the movable short and the experiment was carried out for three charge conditions at the junction, namely charge maximum, charge minimum and a case in between maximum and minimum. The experiment was repeated for consistancy. Even though frequency drift was observed, the change in electric length of the test structure was of only of the order of $\pm$ 0.001λ which was considered negligible. Any change in the power output of the oscillator was compensated for by monitoring the oscillator output using a broadband sampling meter.

Care was taken while making the probe to see that the top of the probe carriage fits flush with the test structure. To achieve good electrical contact between the probe carriage and the test structure, silver conducting grease (Eccoshield, manufactured by Emerson & Cuming)

was applied along the sides of the probe carriage and the sidewalls of the probe. The signal carrying probe tube was coated with an absorber (Eccosorb by Emerson & Cuming) to avoid the possibility that the probe tube would become the center conductor of a TEM structure inside of the inner conductor of the test structure and give rise to propagation and unwanted resonances.

After obtaining the extrapolated value of the probe reading at the junction the probe calibration factor was obtained as described in the following section.

(iv) Determination of Probe Calibration Factor

Let P_1 and P_2 be the probe reading obtained by extrapolating the measured data to the junction of the large and small tubes of radii a_1 and a_2. Let N_1 and N_2 be the normalizing factors.

$$P_1 = N_1 \eta_1 \qquad (2.10)$$

$$P_2 = N_2 \eta_2 \qquad (2.11)$$

therefore

$$\frac{\eta_1}{\eta_2} = \frac{P_1}{P_2} \frac{N_2}{N_1}$$

from eq. (2.9)(b) the ratio of $\dfrac{\eta_1}{\eta_2}$ is given by,

$$\frac{\eta_1}{\eta_2} = \frac{a_2}{a_1} \frac{\ln\left(\frac{b}{a_2}\right)}{\ln\left(\frac{b}{a_1}\right)}$$

21

The probe calibration factor, $\dfrac{N_1}{N_2}$ is then given by,

$$\frac{N_1}{N_2} = \frac{P_1}{P_2} \frac{a_1}{a_2} \frac{\ln\left(\frac{b}{a_1}\right)}{\ln\left(\frac{b}{a_2}\right)} \tag{2.12}$$

(v) Curve Fitting: Modified Prony's Method

The experimental data obtained has magnitude and phase so that it is a complex quantity. Curve fitting to the experimental data is done by using a modified Prony's method. Prony's method [7] fits a set of data to a series of exponentials. By assuming a function of the form

$$f(z) = A_1 e^{\gamma z} + A_2 e^{-\gamma z} \tag{2.13}$$

because of the TEM mode transmission, only two terms are selected from the exponential series of the general Prony's method with

$$\gamma = (\alpha + j\,\beta) \tag{2.14}$$

where α is the attenuation constant, β is the propagation constant.

$$f(z) = A_1 e^{(\alpha+j\beta)z} + A_2 e^{-(\alpha+j\beta)z} \tag{2.15}$$

where A_1 and A_2 are complex constants, A_1, A_2, α, β are to be determined.

Let Δz be the spacing between the data points and

$$u_1 = e^{\gamma \Delta z} \tag{2.16}$$

$$u_2 = e^{-\gamma \Delta z} \tag{2.17}$$

22

then
$$f_{k+1}(k\Delta z) = A_1 u_1{}^k + A_2 u_2{}^k \qquad (2.18)$$

Assume u_1 and u_2 are two roots of

$$u^2 + \alpha_1 u + \alpha_0 = 0 \qquad (2.19)$$

where α_0 and α_1 are unknown.

Equation (2.18) can be expanded to

$$f_1 = A_1 + A_2 \qquad (2.18)(a)$$

$$f_2 = A_1 u_1 + A_2 u_2 \qquad (2.18)(b)$$

$$f_3 = A_1 u_1{}^2 + A_2 u_2{}^2 \qquad (2.18)(c)$$

$$f_k = A_1 u_1{}^{k-1} + A_2 u_2{}^{k-1} \qquad (2.18)(d)$$

Since the above set of equations satisfy equation (2.19)

$$f_3 + f_2 \alpha_1 + f_1 \alpha_0 = 0$$

$$f_4 + f_3 \alpha_1 + f_2 \alpha_0 = 0$$

The unknowns α_0, α_1 can be determined from the above equations. Once α_0, α_1 are known, the roots u_1, u_2 can be determined from equations (2.19). Once u_1 and u_2 are known, γ may be obtained from equations (2.16) or (2.17) or,

$$\gamma = \ln(u_1)/\Delta z \qquad (2.20)$$

$$-\gamma = \ln(u_2)/\Delta z \qquad (2.21)$$

23

With γ known A_1 and A_2 are then determined from (2.18)(a) and (2.18)(b). Since the roots u_1 and u_2 are reciprocal by definition, $u_2 = \frac{1}{u_1}$. Substituting in (2.19) we get

$$u_1^2 + \alpha_1 u_1 + \alpha_0 = 0$$

$$\frac{1}{u_2^2} + \alpha_1 \frac{1}{u_2} + \alpha_0 = 0 \tag{2.22}$$

$$1 + \alpha_1 u_2 + \alpha_0 u_2^2 = 0 \tag{2.23}$$

Comparing (2.19) and (2.23) we obtain,

$$\alpha_0 = 1$$

$$u^2 + \alpha_1 u + 1 = 0 \tag{2.24}$$

If we determine α_1, then the roots can be found easily in the following way,

$$f_1 + f_2 \alpha_1 + f_3 = 0 \qquad ; \qquad f_2 \alpha_1 = -(f_1 + f_3)$$

$$f_2 + f_3 \alpha_1 + f_4 = 0 \qquad ; \qquad f_3 \alpha_1 = -(f_2 + f_4)$$

$$f_3 + f_4 \alpha_1 + f_5 = 0 \qquad ; \qquad f_4 \alpha_1 = -(f_3 + f_5)$$

With three datapoints one can easily determine α_1 from which u_1 and u_2 can be determined.

The method described so far is not satisfactory for the set of data where experimental noise is present. A larger number of datapoints

is used and a least square curve fitting technique is employed.

Let $M\Delta z$ be the spacing between datapoints. When $3M=N$, where N is the total number of datapoints,

$$f_1 + f_{m+1}\alpha + f_{2m+1} = 0 \quad ; \quad f_{m+1}\alpha = -(f_1 + f_{2m+1})$$

$$f_2 + f_{m+2}\alpha + f_{2m+2} = 0 \quad ; \quad f_{m+2}\alpha = -(f_2 + f_{2m+2})$$

$$f_3 + f_{m+3}\alpha + f_{2m+3} = 0 \quad ; \quad f_{m+3}\alpha = -(f_3 + f_{2m+3})$$

$$f_m + f_{2m}\alpha + f_{3m} = 0 \quad ; \quad f_{2m}\alpha = -(f_m + f_{3m})$$

In general

$$[F]\alpha = -(G)$$

$$[F^T F]\alpha = -[F^T][G]$$ where $[F^T]$ is the transpose matrix of $[F]$

Therefore $\alpha = - [F^T F]^{-1} [F^T] [G]$ (2.25)

The residues A_1 and A_2 can be determined in the following way

$$f_1 = A_1 + A_2$$

$$f_2 = A_1 e^{\gamma\Delta z} + A_2 e^{-\gamma\Delta z}$$

$$f_N = A_1 (e^{\gamma\Delta z})^{N-1} + A_2 (e^{-\gamma\Delta z})^{N-1}$$

$$[F] = [G][A]$$

$$[A] = [G^T G]^{-1} [G^T] [F]$$ (2.26)

With A_1, A_2, γ_1 and γ_2 thus determined, a continuous curve may then be computed from equation (2.15) and extrapolated to the junction. The value of P_1 and P_2 in equation (2.12) were obtained by this procedure.
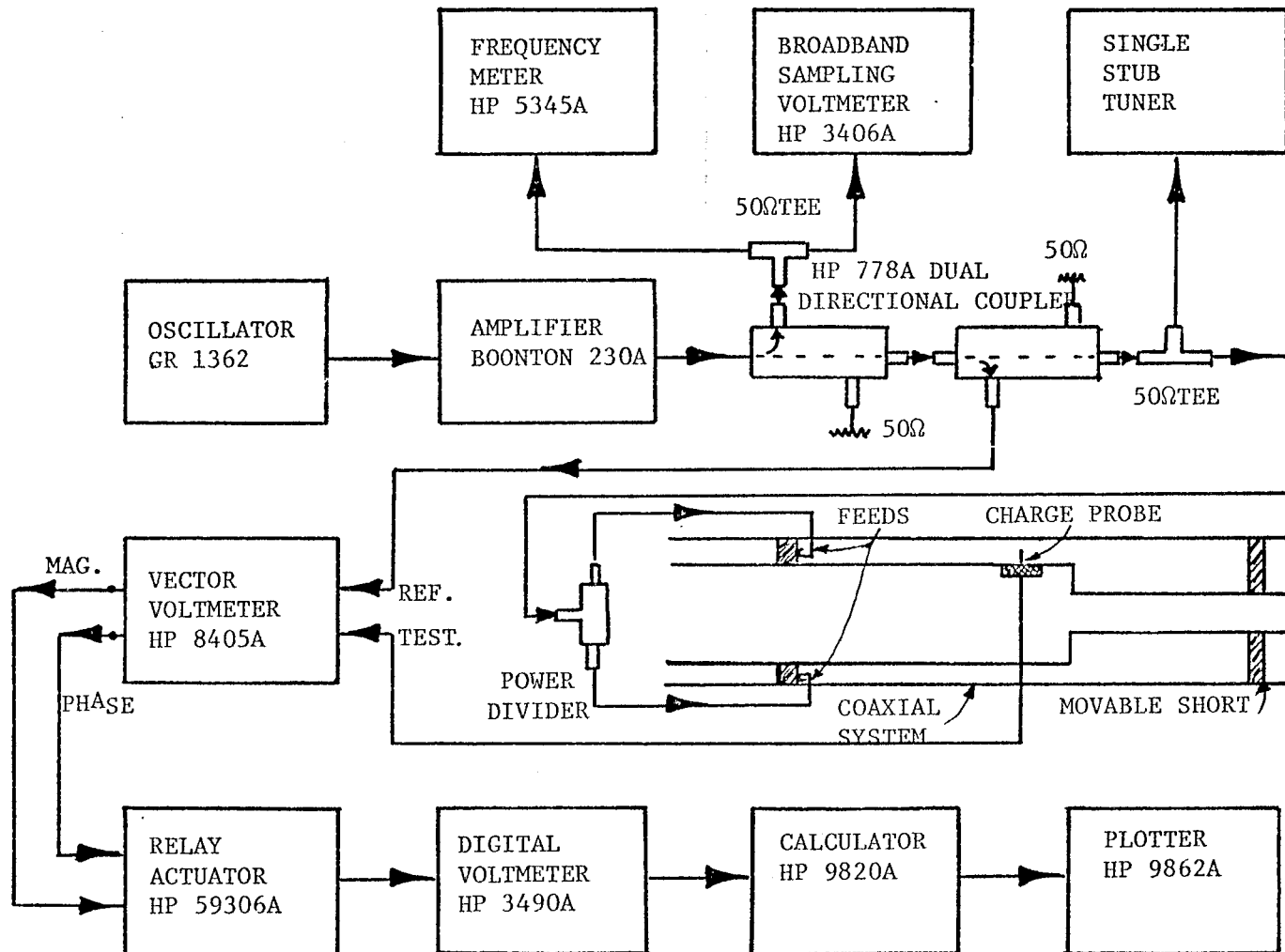
Fig. (2.6) BLOCK DIAGRAM OF MEASUREMENT SYSTEM.

CHAPTER III

NUMERICAL ANALYSIS

(i) Charge Probe as a Scatterer: Theory and Solution

The preceding chapter discussed the experimental determination of
the response of a charge probe. A theoretical analysis and numerical
solution for the probe response and calibration factor are presented
in the present chapter. For the purpose of this analysis, the probe
is modeled as a monopole scatterer perpendicular to an infinite plane
conductor and planar image theory is employed. As discussed in
Chapter II the major effect of the cylindrical conductor upon which
the probe is mounted is the $\frac{1}{\rho}$ variation of the $\bar{E}$ field produced by
the charge on the test structure. In the treatment of the probe as a
scatterer the correct $\frac{1}{\rho}$ dependence of the incident field is imposed.
It is recognized, however, that some error is introduced by using
planar image theory rather than the Green's function for a source ex-
terior to a cylindrical conductor.

From the specification given in Chapter II, for the cable from
which the probe is constructed, the electrical radius, ka, is found to
be .00036 for an operating frequency of 300 MHz. It is therefore
appropriate to make the usual thin wire approximations.

(ii) Formulation of Straight Wire Integral Equation

The charge probe of length $\frac{H}{2}$ slides in a charged conductor of radius a_1 in a homogeneous medium characterised by (μ, ε, $\sigma = 0$) is shown in Fig. (3.1). The z axis of a cylindrical coordinate system lies at the center of the charged conductor as shown in Fig. (3.1). The probe is perpendicular to the charged conductor and extends from $\rho = a_1$ to $\rho = a_1 + \frac{H}{2}$. For convenience a coordinate transformation is used with a new variable $\zeta = (\rho - a_1)$ measured along the probe axis as shown in Fig. (3.2).

The current and charge on the probe produce an electric field $\bar{E}^s(\zeta)$ on the probe surface which has a ζ component, $E_\zeta^s(\zeta)$ given by,

$$E_\zeta^s(\zeta) = \frac{-j\omega}{k^2} \left(\frac{\partial^2}{\partial \zeta^2} + k^2\right) A_\zeta(\zeta) \qquad (3.1)$$

where A_ζ is the vector potential evaluated on the probe surface and k is the propagation constant. Since $A_\zeta(\zeta)$ is produced entirely by the current on the probe, it is given by,

$$A_\zeta(\zeta) = \frac{\mu}{4\pi} \int_{\zeta'=-H/2}^{H/2} I_\zeta(\zeta') K(\zeta-\zeta') d\zeta' \qquad (3.2)$$

where $I_\zeta(\zeta)$ is the total axial current on the probe and

$$K(\zeta-\zeta') = \frac{1}{2\pi} \int_{\psi'=-\pi}^{+\pi} \frac{e^{-jk[(\zeta-\zeta')^2 + 4a^2 \sin^2(\frac{\psi'}{2})]^{\frac{1}{2}}}}{[(\zeta-\zeta')^2 + 4a^2 \sin^2(\frac{\psi'}{2})]^{\frac{1}{2}}} \, \partial \psi' \qquad (3.3)$$
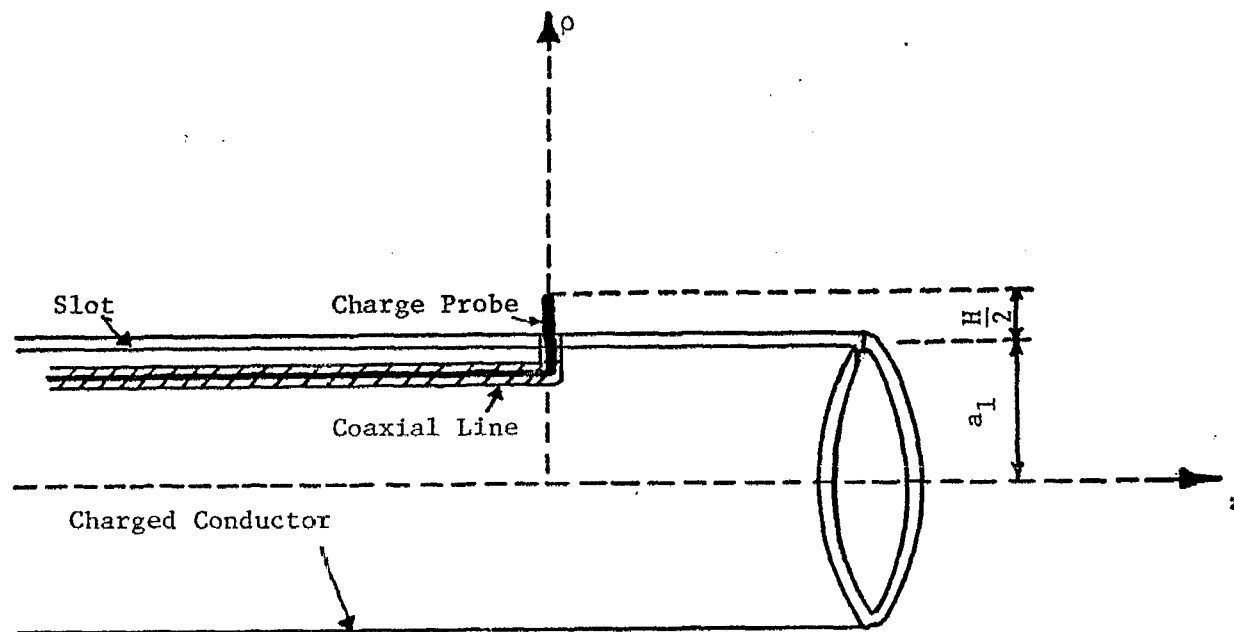
Fig. (3.1)   CHARGE PROBE ON A CHARGED CONDUCTOR.
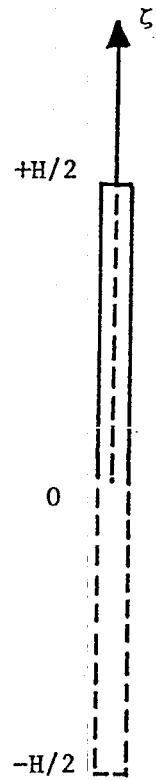
Fig. (3.2)   CHARGE PROBE AS
            A SCATTERER.
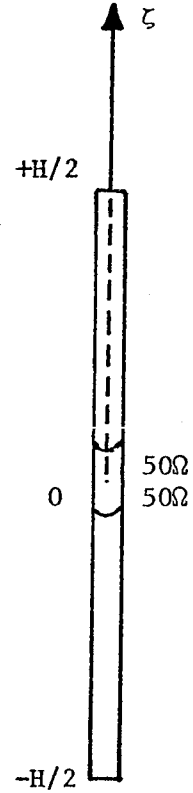
Fig. (3.3)   LUMPED LOAD Z_{LOAD} AT $\zeta = 0$.
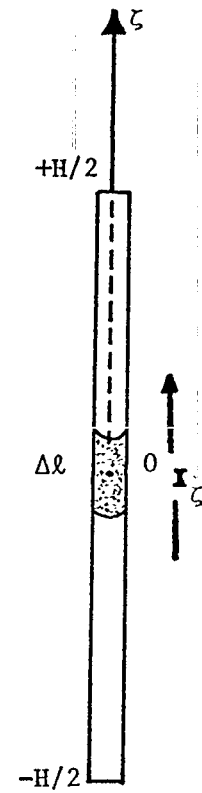
where a = radius of probe, and ψ = angle variable of a cylindrical

coordinate system with ζ as the axis.

Applying the boundary condition that the tangential electrical

field on the probe surface be zero, we obtain,

$$E_\zeta^i(\zeta) + E_\zeta^s(\zeta) = 0$$

and therefore

$$E_\zeta^i(\zeta) = -E_\zeta^s(\zeta)$$

Thus the integro-differential equation becomes,

$$\frac{j\omega}{k^2} \left(\frac{\partial^2}{\partial\zeta^2} + k^2 \right) A_\zeta(\zeta) = E_\zeta^i(\zeta) \qquad (3.4)$$

(iii) Charge Probe with 50 Ω Load

The charge probe sees the 50 Ω input impedance of the coaxial

cable, so that loading on the probe should be considered. For a

lumped load of impedance Z_{load} inserted at $\zeta = 0$ as illustrated in

Fig. (2.3), the current I_ζ in Z_{load} causes a scalar potential drop

$\Delta\phi_\ell$ across the load of

$$\Delta\phi_\ell = I_\zeta(0) \cdot Z_{load}$$

The approximate electric field on the surface of the load element ,

which must be added to the $\bar{E}^s$ is,

$$E_\zeta(0) = \frac{\Delta\phi_\ell}{\Delta\ell} = I_\zeta(0) \, Z_{load} \, \frac{1}{\Delta\ell}$$

To achieve more useful representation for the electric field due

to the I_ζ in Z_{load}, we look upon the effect of the load at $\zeta = 0$ as a

local behavior at $\zeta = 0$ and write,

$$E_\zeta(0) = I_\zeta(0) \, Z_{load} \cdot \delta(\zeta)$$

In the case of a scatterer,

$$\frac{j\omega}{k^2} \left(\frac{\partial^2}{\partial \zeta^2} + k^2 \right) A_\zeta(\zeta) + I_\zeta(0) \cdot Z_{load} \, \delta(\zeta) = E_\zeta^i(\zeta) \tag{3.5}$$

As explained in the beginning $E_\zeta^i(\zeta)$ has been selected to be proportional to $\frac{1}{\rho}$ where $\rho = (\zeta + a_1)$. Equation (3.5) with (3.2) is the final form of the integral equation for the probe current. Equation (3.5) has been solved numerically by the method described in the next section.

(iv) Numerical Solution Technique

In this section a technique for solving the integro-differential equation is presented. This technique uses piecewise linear testing and pulse expansion. One performs the testing of the equation to be solved with elements t_m of the selected testing set $\left\{ t_m \right\}$ before the unknown current is approximated as a linear combination of the elements i_n of the basis set $\left\{ i_n \right\}$.

Leading to the numerical solution of equation (3.5), one equates the corresponding projections of the two sides of (3.5) onto the space spanned by $\left\{ t_m \right\}$ which implies that the scalar products formed by t_m and two sides of (3.5) are equated for each m. The piecewise linear testing scheme is shown in Fig. (3.4)

33
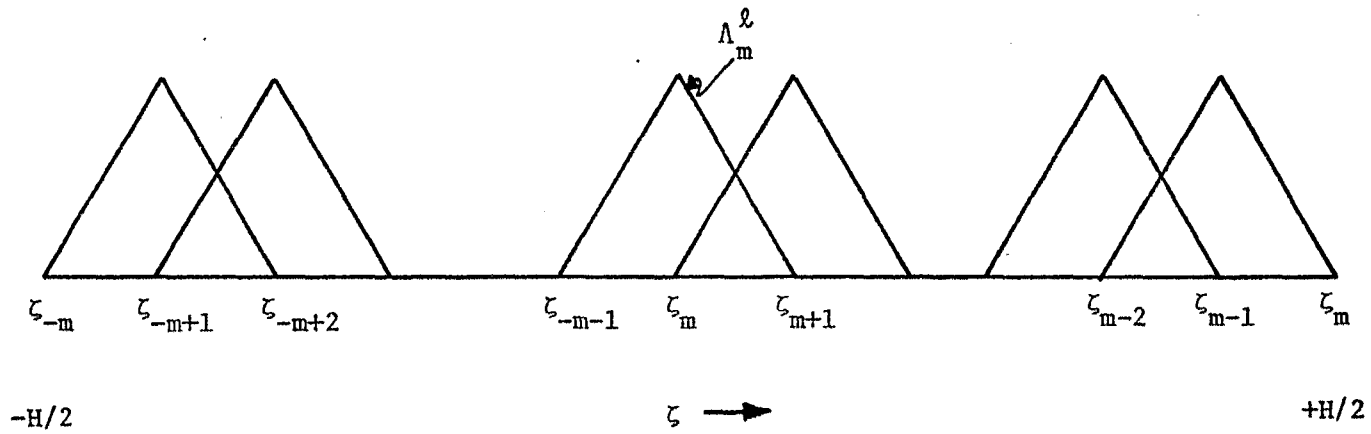
Fig. (3.4)   TRIANGLES IN PIECEWISE LINEAR TESTING SCHEME.

$$\left\langle \frac{j\omega}{k^2} \left(\frac{\partial^2}{\partial\zeta^2} + k^2\right) A_\zeta + Z_{load} I_\zeta(0)\delta(\zeta), t_m \right\rangle = \left\langle E_\zeta^i, t_m \right\rangle \qquad (3.6)(a)$$

where the scalar product is

$$\langle f, g \rangle = \int_{\zeta=-H/2}^{+H/2} f \, g^* \, d\zeta \qquad (3.6)(b)$$

For a real testing set $\{t_m\}$ of the subdomain type considered here where $t_m(\zeta)$ is zero outside

$$\zeta \in (\zeta_{m-1}, \zeta_{m+1})$$

Equation (3.6) becomes

$$\frac{j\omega}{k^2} \int_{\zeta=\zeta_{m-1}}^{\zeta_{m+1}} \left(\frac{\partial^2}{\partial\zeta^2} + k^2\right) A_\zeta(\zeta) \, t_m(\zeta) \, d\zeta + \int_{\zeta=\zeta_{m-1}}^{\zeta_{m+1}} I_\zeta(0) \, Z_{load}\delta(\zeta) \, t_m(\zeta) \, d\zeta$$

$$= \int_{\zeta=\zeta_{m-1}}^{\zeta_{m+1}} E_\zeta^i(\zeta) \, t_m(\zeta) \, d\zeta \qquad (3.7)$$

Setting $t_m = \Lambda_m^\ell = \dfrac{\Delta - |\zeta - \zeta_m|}{\Delta}$ $\qquad (3.8)$

in the above, the equation becomes

$$\frac{j\omega}{k^2} \left[\frac{1}{\Delta} \left(A_\zeta(\zeta_{m+1}) - 2A_\zeta(\zeta_m) + A_\zeta(\zeta_{m-1}) \right) + k^2 \int_{\zeta=\zeta_{m-1}}^{\zeta_{m+1}} A_\zeta(\zeta)\Lambda_m^\ell(\zeta) \, d\zeta \right]$$

$$+ \int_{\zeta=\zeta_{m-1}}^{\zeta_{m+1}} I_\zeta(0) \, Z_{load} \, \delta(\zeta)\Lambda_m^\ell(\zeta) \, d\zeta = \int_{\zeta=\zeta_{m-1}}^{\zeta_{m+1}} E_\zeta^i(\zeta)\Lambda_m^\ell(\zeta) \, d\zeta \qquad (3.9)$$

with $m = 0 \pm 1, \pm 2, \pm 3, \pm 4, .., \pm (M-1)$ (3.10)(a)

and $2\Delta = (\zeta_{m+1} - \zeta_{m-1})$ (3.10)(b)

For a function f sufficiently smooth over the interval $(\zeta_{m-1}, \zeta_{m+1})$ one employs the approximation

$$\int_{\zeta=\zeta_{m-1}}^{\zeta_{m+1}} f(\zeta) \wedge_m^\ell (\zeta) d\zeta = \Delta f(\zeta_m)$$ (3.11)

The final equation becomes

$$\frac{j\omega}{k^2} (\frac{1}{\Delta}) [A_\zeta(\zeta_{m+1}) - 2(1-\frac{(k\Delta)^2}{2}) A_\zeta(\zeta_m) + A_\zeta(\zeta_{m-1})]$$

$$+ \Delta \, Z_{load} \, I_\zeta(0) \delta_{0m} = \Delta E_\zeta^i (\zeta_m)$$ (3.12)

where δ_{mn} is the kronecker delta

$$\delta_{mn} = \begin{cases} 1, & m=n \\ 0, & m \neq n \end{cases}$$

$m = 0, \pm 1, \pm 2, \pm 3, \pm 4, ..., \pm (M-1)$

(v) Expansion of Current and Formulation of Matrix

The current I_ζ is represented by expanding in known expansion functions each weighted with an unknown coefficient. These unknown coefficients ultimately determine I_ζ. In terms of a pulse basis set, $\{p_n\}$, as the known functions and the complex unknown coefficients I_n, the current becomes

36

$$I_\zeta(\zeta) = \sum_{n=-N}^{N} I_n P_n(\zeta) \tag{3.13}$$

The pulse arrangement for approximating the current on straight wire is shown in Fig. (3.5).

The vector potential can be written as

$$A_\zeta(\zeta) = \sum_{n=-N}^{N} I_n A_{\zeta n}(\zeta) \tag{3.14}$$

where

$$A_{\zeta n}(\zeta) = \frac{\mu}{4\pi} \int_{\zeta'=-H/2}^{H/2} P_n(\zeta') K(\zeta-\zeta') d\zeta' \tag{3.15}$$

is a partial vector potential contributed by the pulse basis element $P_n(\zeta)$. In convenience, the following quantities are defined:

$$Z_{mn} = \frac{j\omega}{k^2} \left(\frac{1}{\Delta}\right) \frac{\mu}{4\pi} \int_{\zeta'=\zeta_{n-\Delta/2}}^{\zeta_{n+\Delta/2}} \left[K(\zeta_{m+1}-\zeta') - 2\left(1-\frac{(\Delta)^2}{2}\right)K(\zeta_m-\zeta') \right.$$

$$\left. + K(\zeta_{m-1}-\zeta') \right] d\zeta' + \Delta\, Z_{load} \zeta_{0m} P_n(\zeta_m) \tag{3.16}(a)$$

$$V_m = \Delta\, E_\zeta^i(\zeta_m) \tag{3.16}(b)$$

In terms of the above definition equation (3.12) becomes

$$\sum_{n=-N}^{N} Z_{mn} I_n = V_m \qquad m=0, \pm 1, \pm 2, \ldots, \pm (M-1) \tag{3.17}$$

37
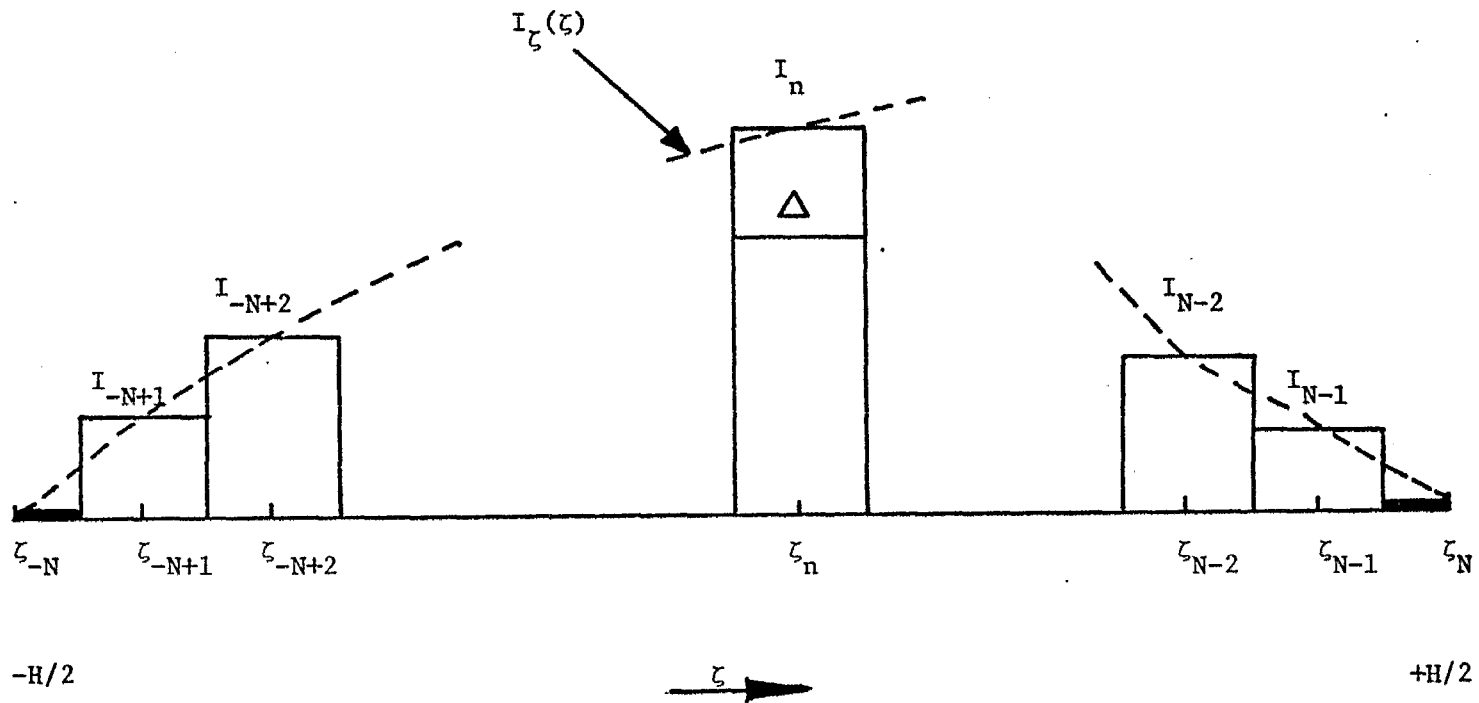
Fig. (3.5)   PULSE ARRANGEMENT FOR APPROXIMATING CURRENT ON STRAIGHT WIRE.

38

The boundary condition that the current goes to zero at the ends is incorporated by directly setting $p_{-N} = p_N = 0$. Equation (3.17) can be conveniently written in matrix form as,

$$[Z][I] = [V] \qquad (3.18)$$

Therefore $\qquad [I] = [Z]^{-1}[V]$

The total scheme of testing and expansion is shown in Fig. (3.6).

(vi) Determination of Probe Calibration Factor

Once the current induced in the load can be found as a function of a_1, the probe calibration factor can be determined as follows. Let I_1 be the current induced in the load when the probe is mounted on the larger radius tube and I_2 be the current induced in the load when the probe is mounted on the smaller radius tube, then relating these to surface charge density

$$I_1 = N_1 \eta_1 \qquad (3.19)$$

$$I_2 = N_2 \eta_2 \qquad (3.20)$$

If the linear density of charge is the same for both tubes then

$$q_1 = q_2$$

or

$$2\pi a_1 \eta_1 = 2\pi a_2 \eta_2$$

$$\frac{\eta_1}{\eta_2} = \left(\frac{a_2}{a_1}\right) \qquad (3.21)$$
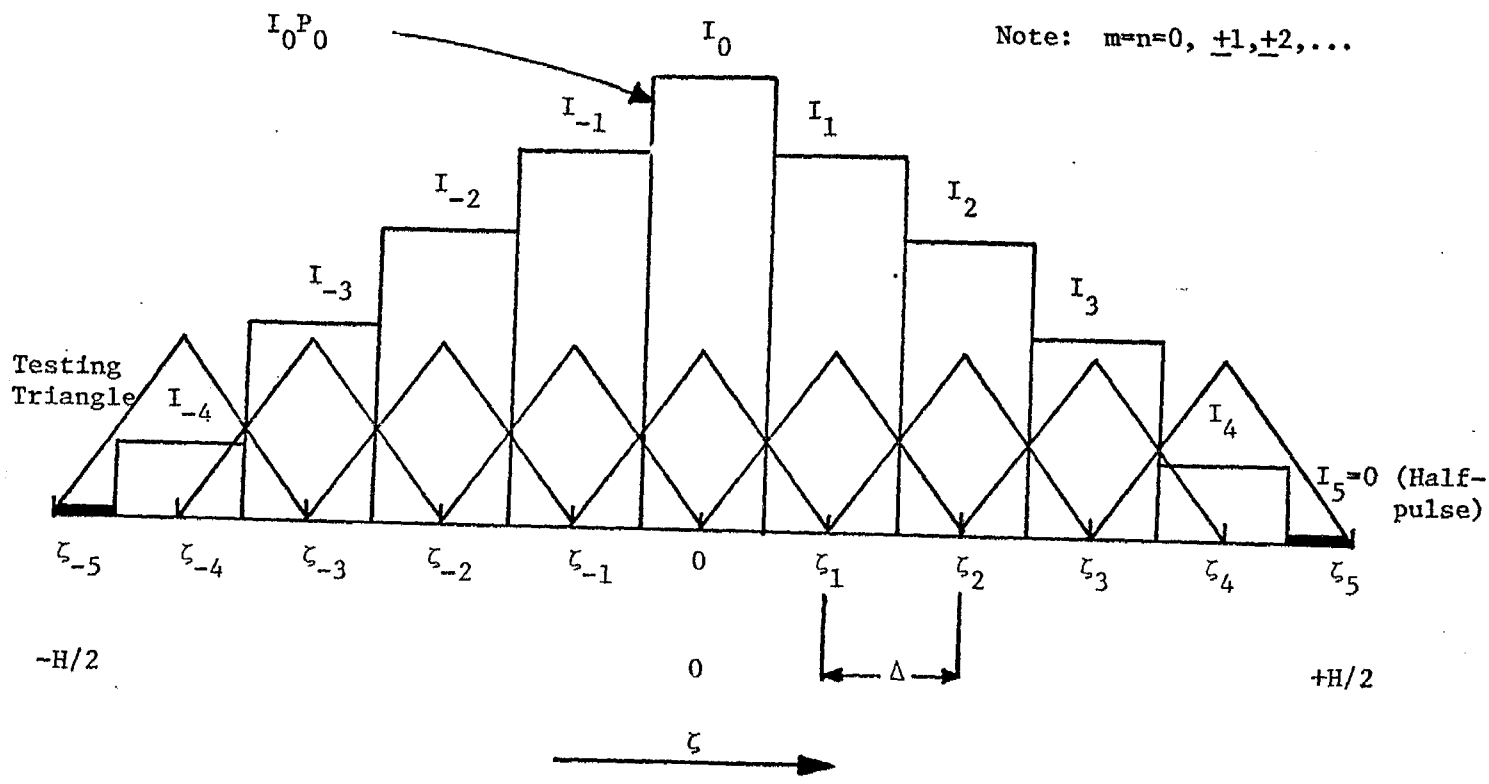
Fig. (3.6)   RELATIVE LOCATIONS OF PULSES (BASES SET) AND TRIANGLES (TESTING SET) ON STRAIGHT WIRE.

From eq. (3.19) and (3.20), the probe calibration factor $\dfrac{N_1}{N_2}$ is obtained as,

$$\frac{N_1}{N_2} = \frac{I_1}{I_2} \cdot \frac{a_1}{a_2} \tag{3.22}$$

The computed value of this ratio for different probe heights for two different radii of cylinders are shown in Fig. (4.19) and (4.20).

CHAPTER IV

PRESENTATION OF DATA AND CONCLUSION

(i) Introduction

Chapter II and III have discussed the measurement technique and
the numerical analysis respectively. It is the purpose of the
present chapter to present the data resulting from both approaches
and discuss these results.

(ii) Measured Data for the Charge Distribution

As explained in Chapter II on measurement the charge density
measurement was made for 3 charge conditions at the junction near
maximum near minimum and a condition in between minimum and maximum.

The figures (4.1) to (4.9) present the charge distribution of
the step radius system with $a_1 = 5/16"$ and $a_2 = 1/8"$ for 3 different
probe heights 0.10", 0.08", and 0.06". For each probe height,
measured data for 3 different charge conditions at the junction are
presented along with the curve determined from the modified Prony's
method for the magnitude of the measured data. Similarly the
Figures (4.10) to (4.18) present the data for the step radius system
with $a_1 = 3/16"$ and $a_2 = 1/8"$.

(iii) Probe Calibration Factor

The probe calibration factor (N_1/N_2) as a function of probe
height as computed from the measured data is shown in Fig. (4.19) for
$a_1 = 5/16"$ and $a_2 = 1/8"$. The theoretical probe calibration factor

CHARGE PROBE RESPONSE: PROBE HEIGHT 0.10"
  ⊙   PHASE   A1 = 5/16"   A2 = 1/8"
  ✳   MAGNITUDE
  ──   CURVE FIT
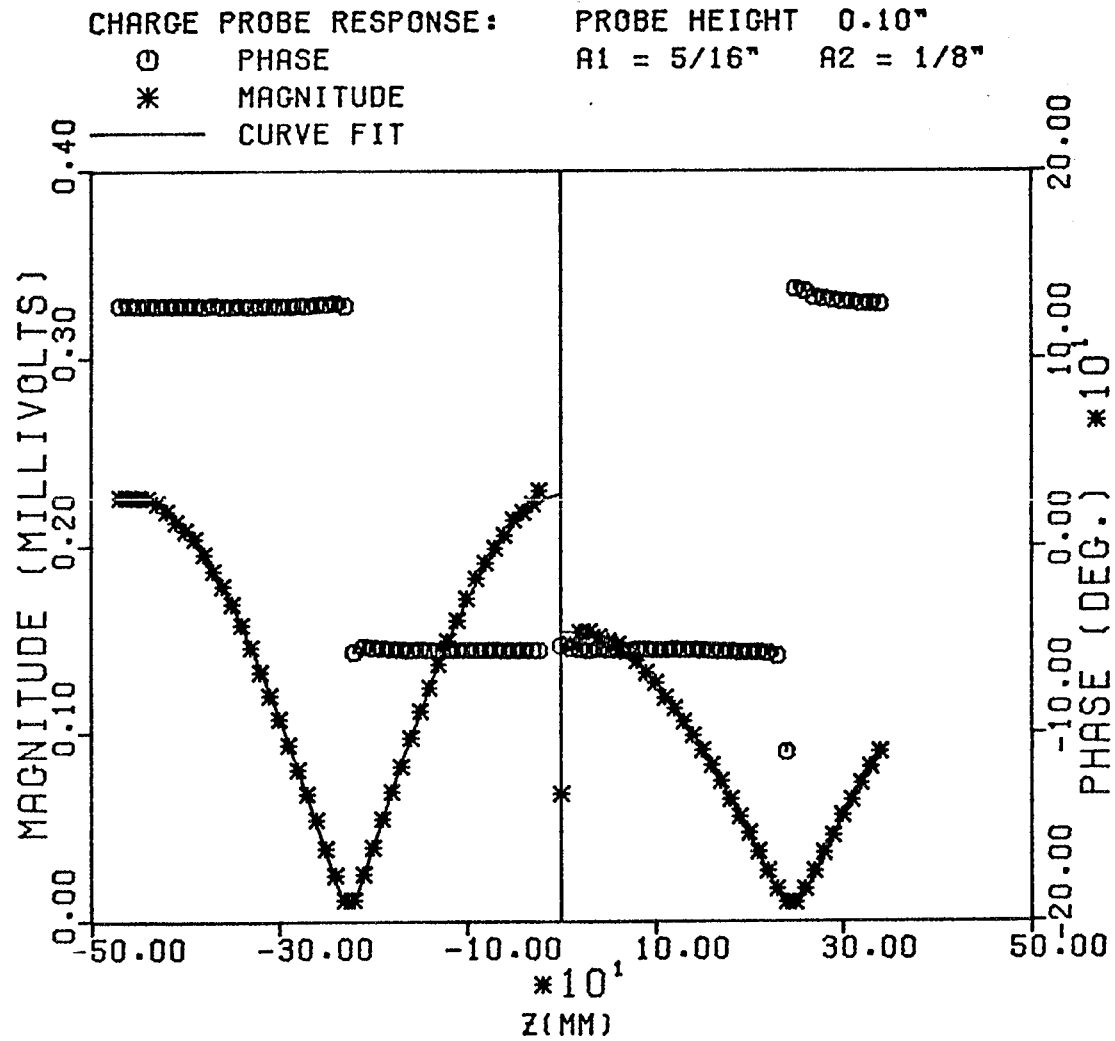
Fig. (4.1)   MAXIMUM CHARGE CONDITION − PROBE HEIGHT = 0.10", a_1= 5/16"

Fig. (4.2) MEDIUM CHARGE CONDITION — PROBE HEIGHT = 0.10", a_1 = 5/16"

CHARGE PROBE RESPONSE: PROBE HEIGHT 0.10"
    ⊙   PHASE   A1 = 5/16"   A2 = 1/8"
    *   MAGNITUDE
    ─── CURVE FIT
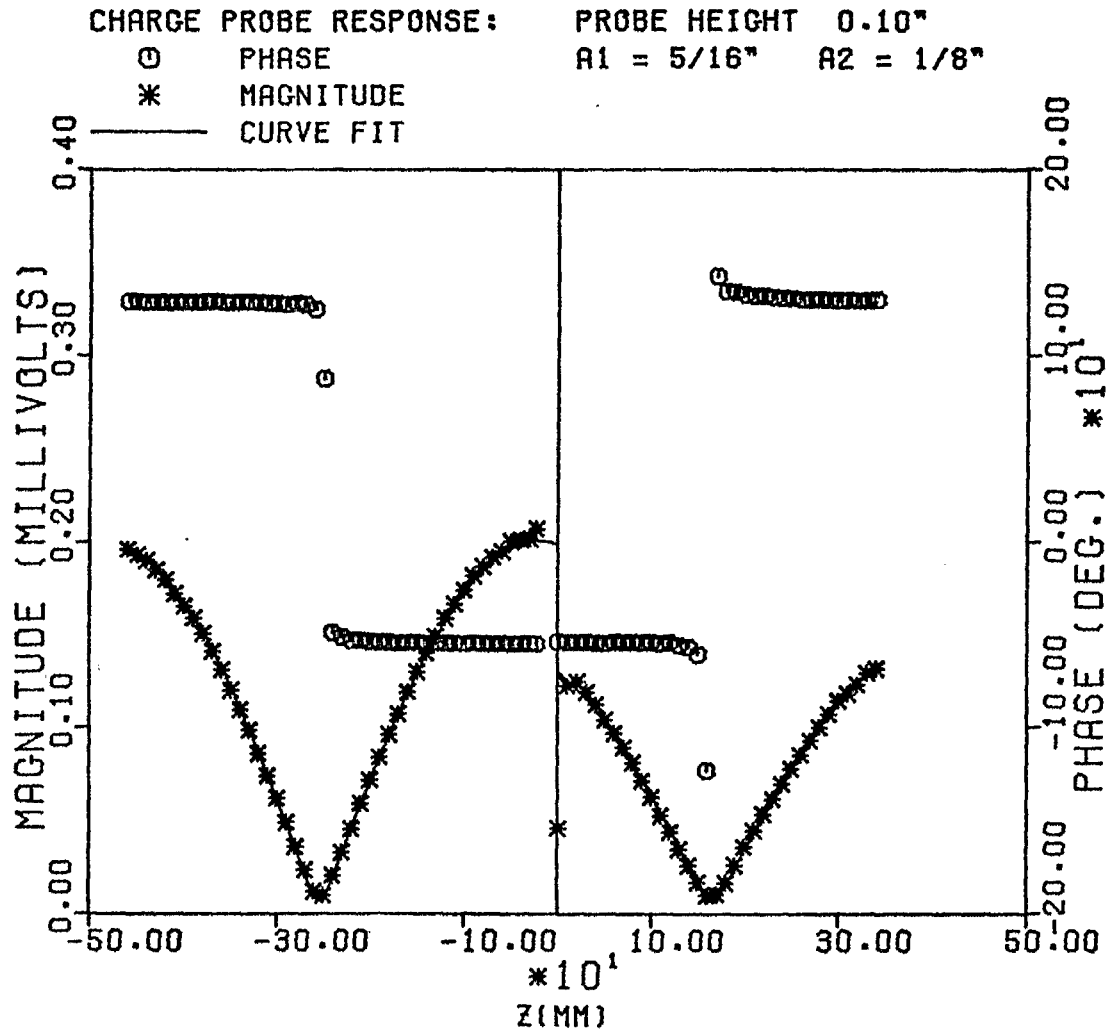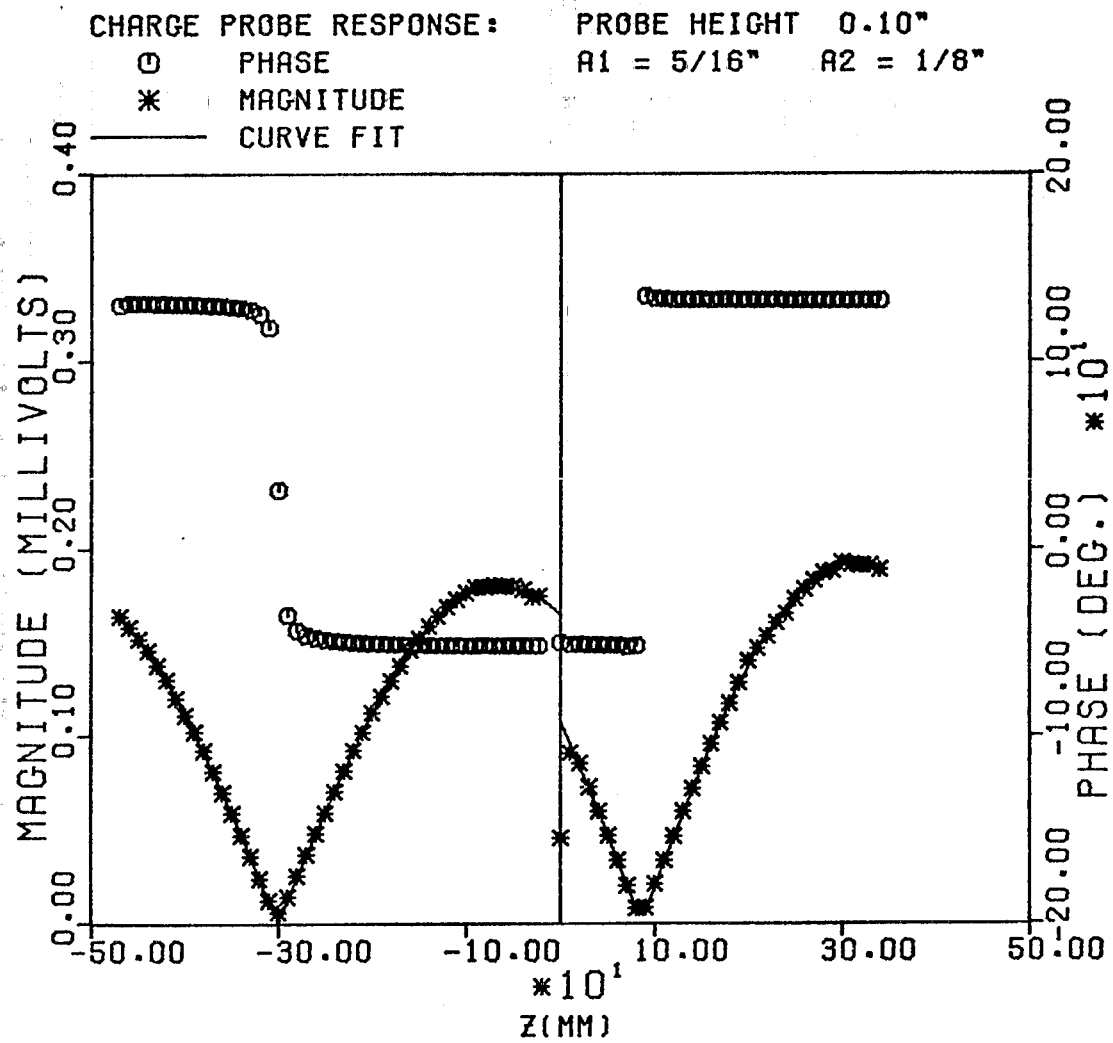
Fig. (4.3)   MINIMUM CHARGE CONDITION — PROBE HEIGHT = 0.10", a_1 = 5/16"

45

Fig. (4.4)   MAXIMUM CHARGE CONDITION − PROBE HEIGHT = 0.08", a_1 = 5/16"

CHARGE PROBE RESPONSE: PROBE HEIGHT 0.08"
    ⊙   PHASE   A1 = 5/16"   A2 = 1/8"
    ✳   MAGNITUDE
   ———   CURVE FIT

Fig. (4.5) MEDIUM CHARGE CONDITION - PROBE HEIGHT = 0.08", a_1 = 5/16"

CHARGE PROBE RESPONSE: PROBE HEIGHT 0.08"
   ⊕   PHASE   A1 = 5/16"   A2 = 1/8"
   ✳   MAGNITUDE
   ——   CURVE FIT
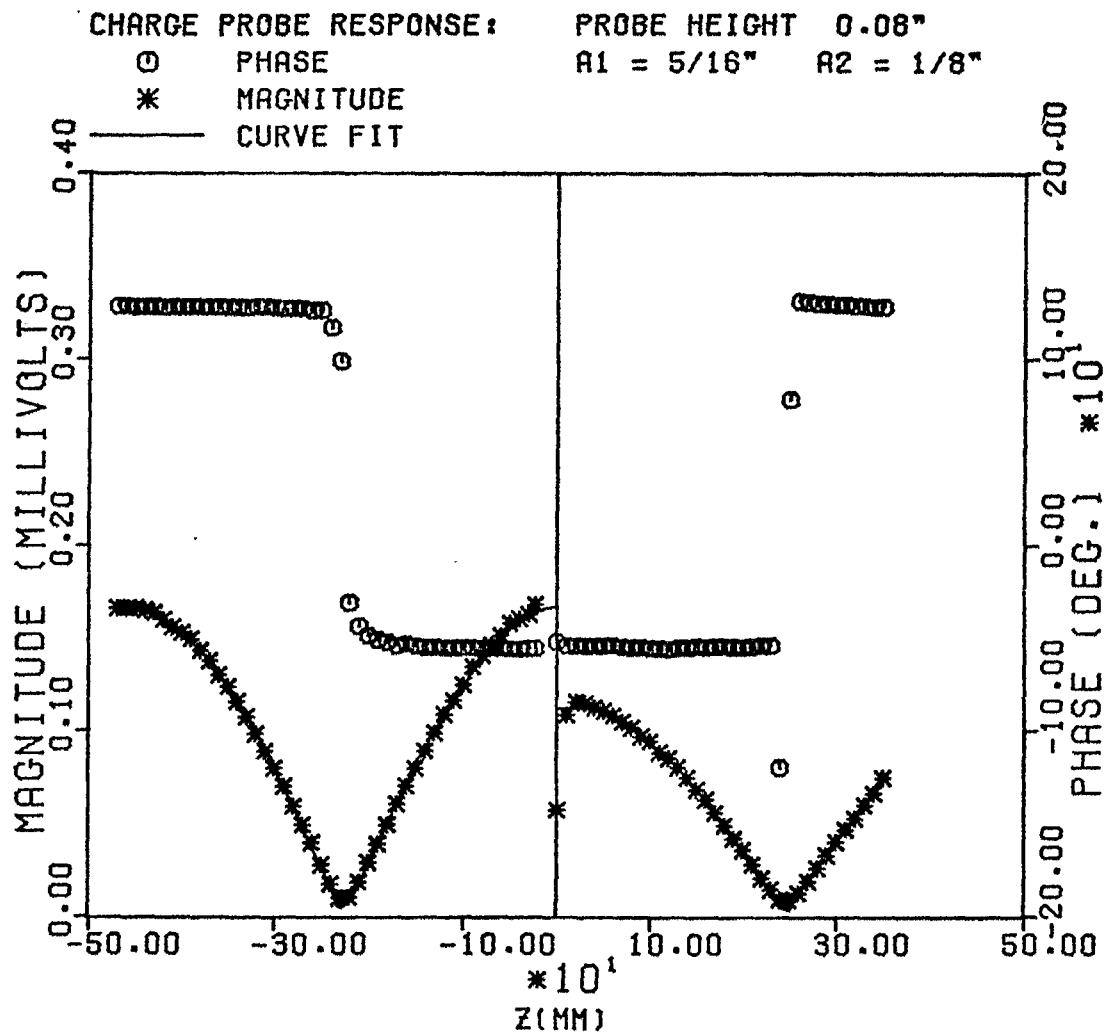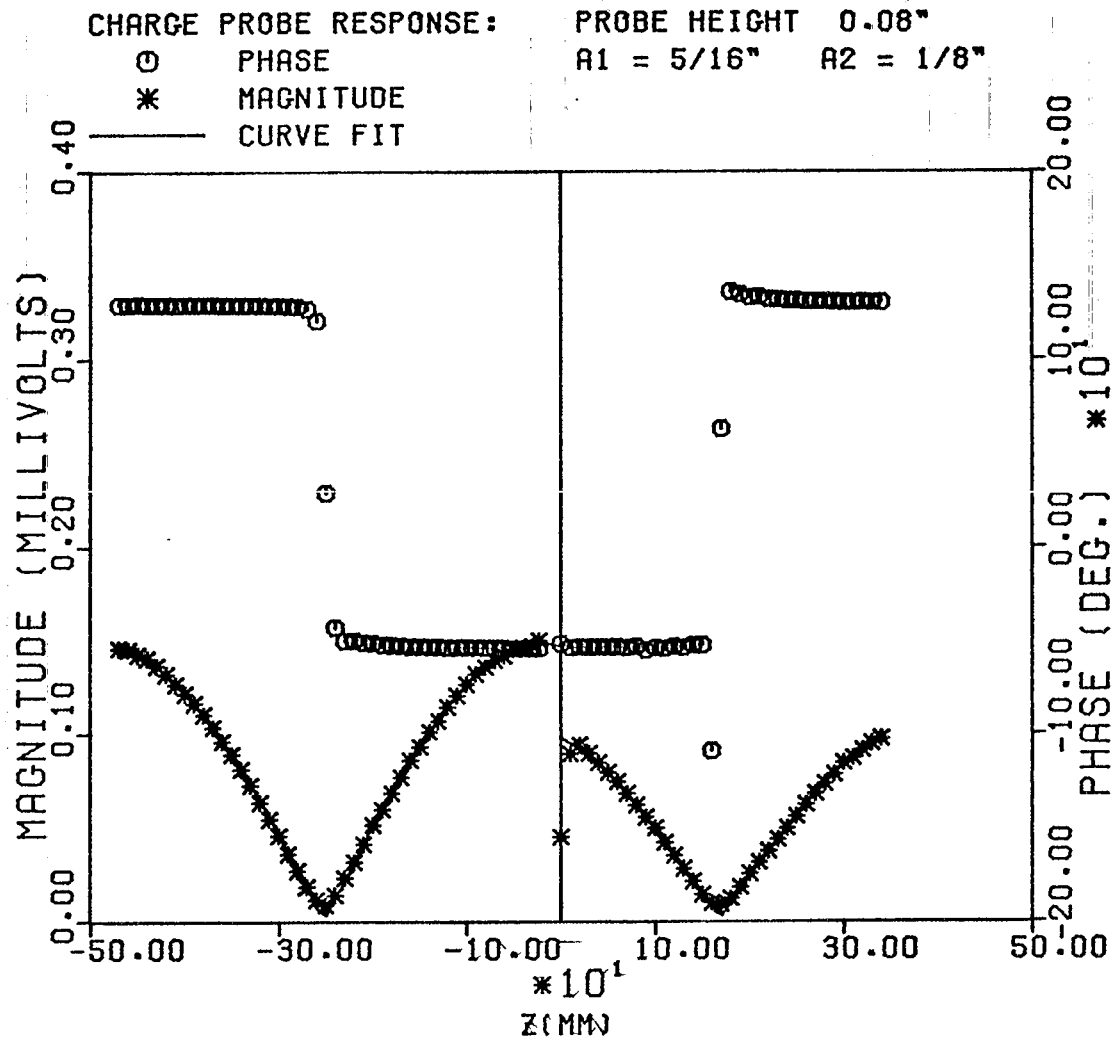
Fig. (4.6)   MINIMUM CHARGE CONDITION - PROBE HEIGHT = 0.08", a_1= 5/16"
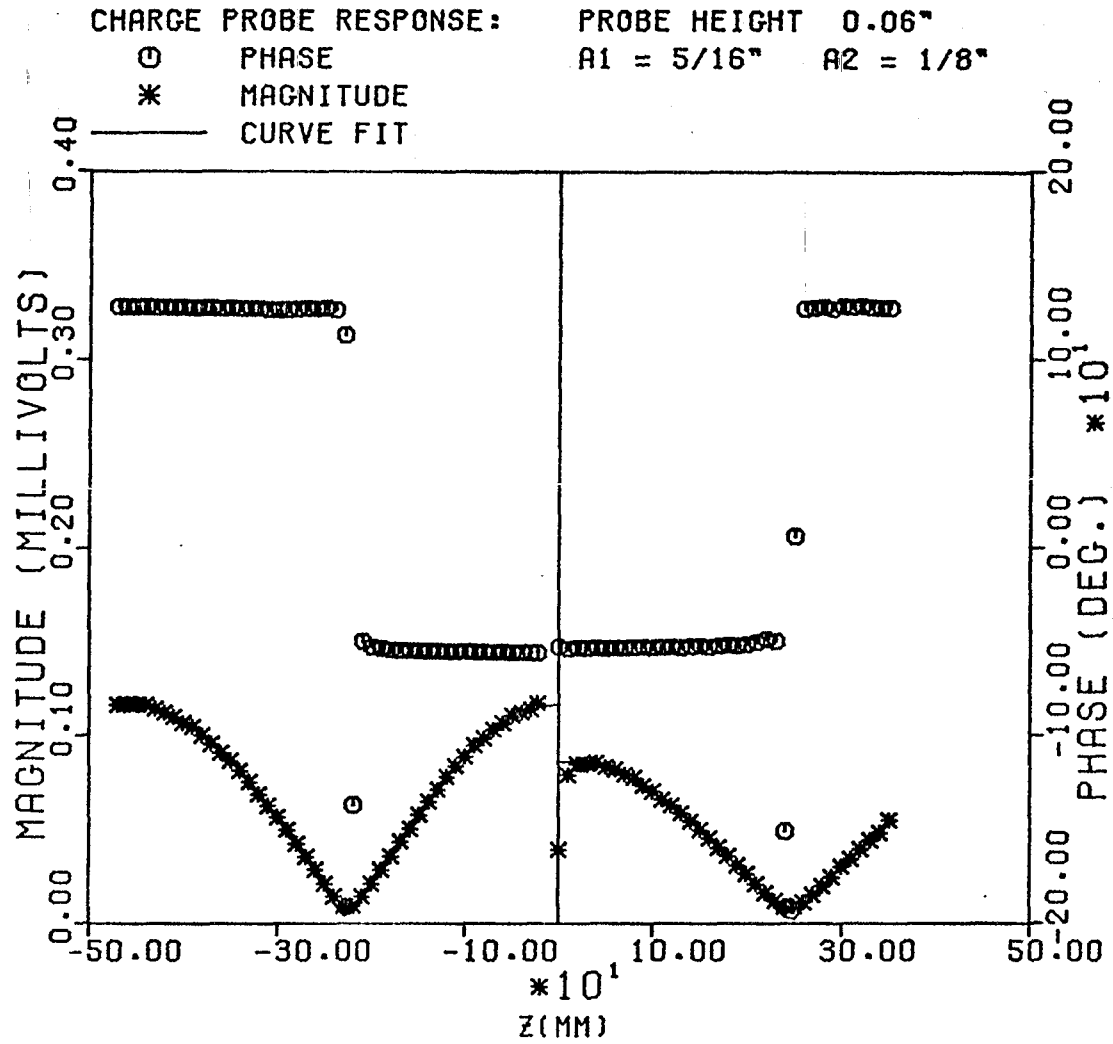
Fig. (4.7) MAXIMUM CHARGE CONDITION - PROBE HEIGHT = 0.06", a_1= 5/16"
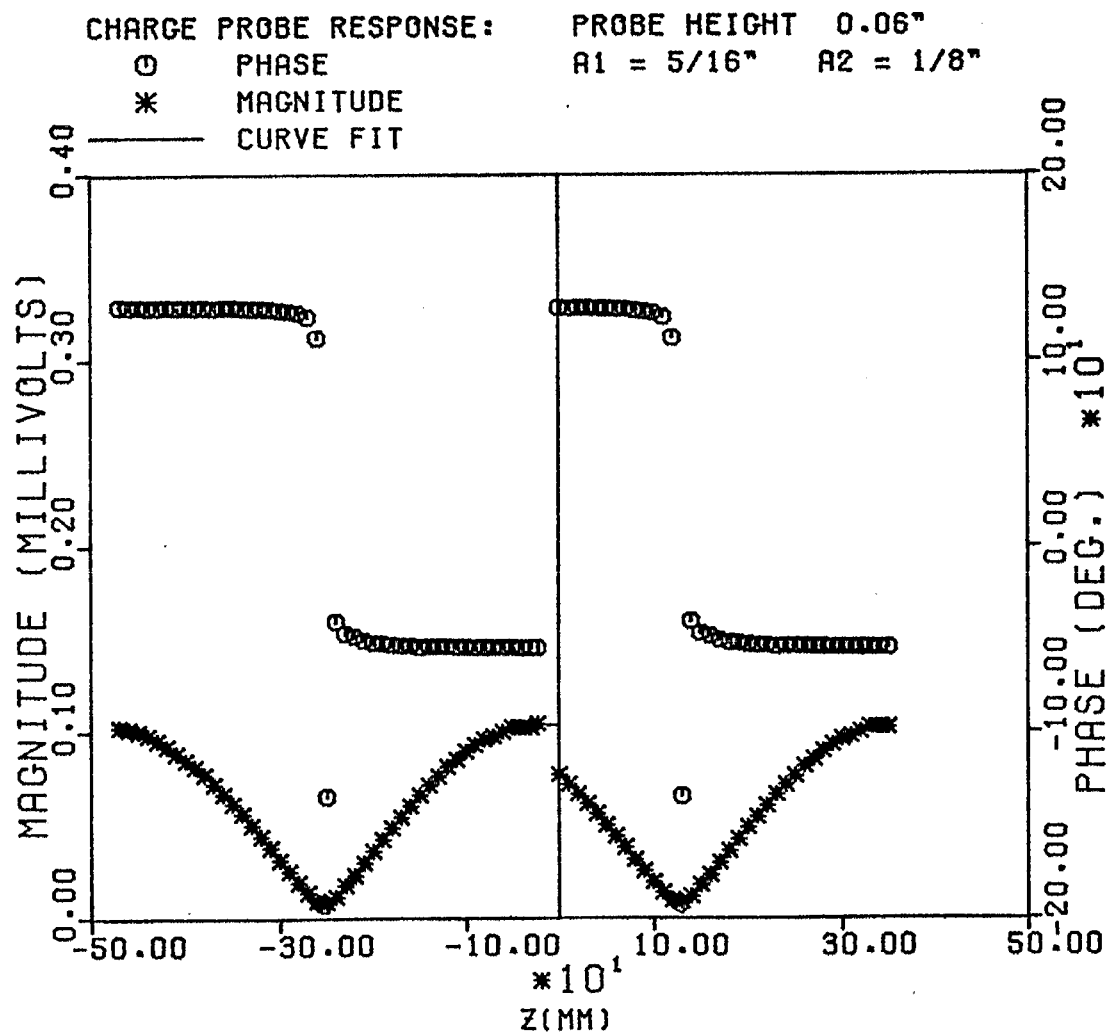
Fig. (4.8)   MEDIUM CHARGE CONDITION – PROBE HEIGHT = 0.06", a_1 = 5/16"
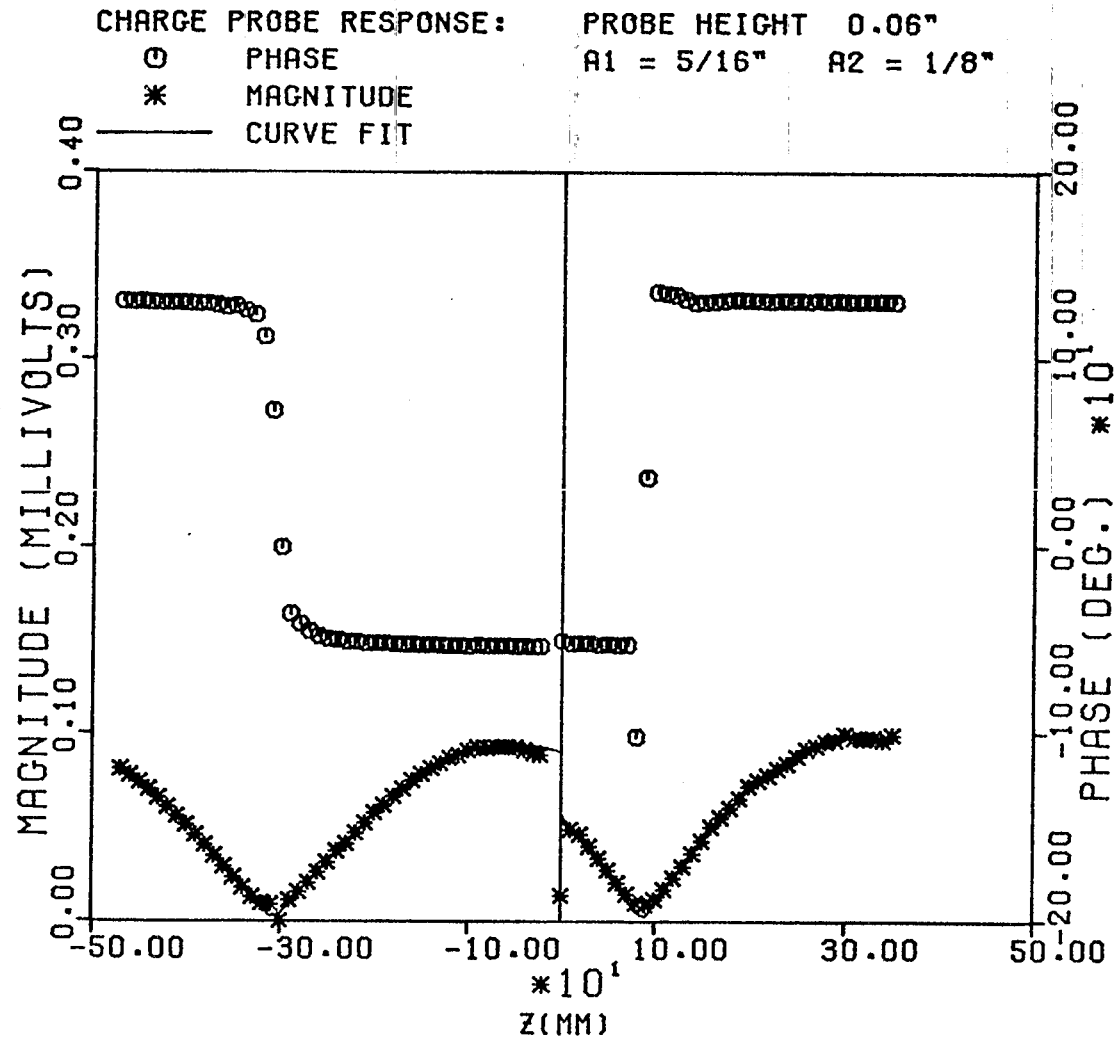
Fig. (4.9) MINIMUM CHARGE CONDITION - PROBE HEIGHT = 0.06", a_1 = 5/16"
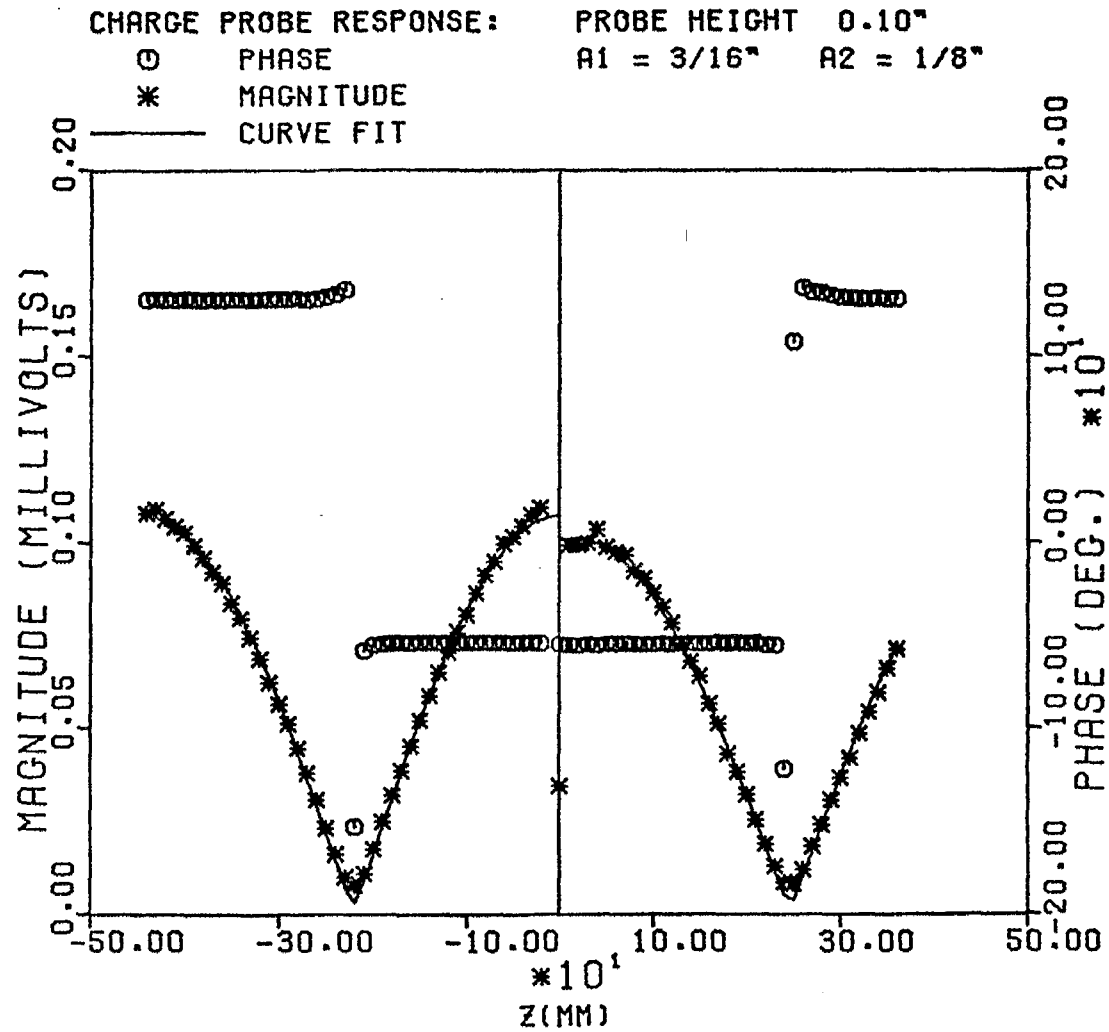
Fig. (4.10)   MAXIMUM CHARGE CONDITION – PROBE HEIGHT = 0.10", a_1= 3/16"

CHARGE PROBE RESPONSE: PROBE HEIGHT 0.10"
    ○   PHASE   A1 = 3/16"   A2 = 1/8"
    *   MAGNITUDE
   ——   CURVE FIT
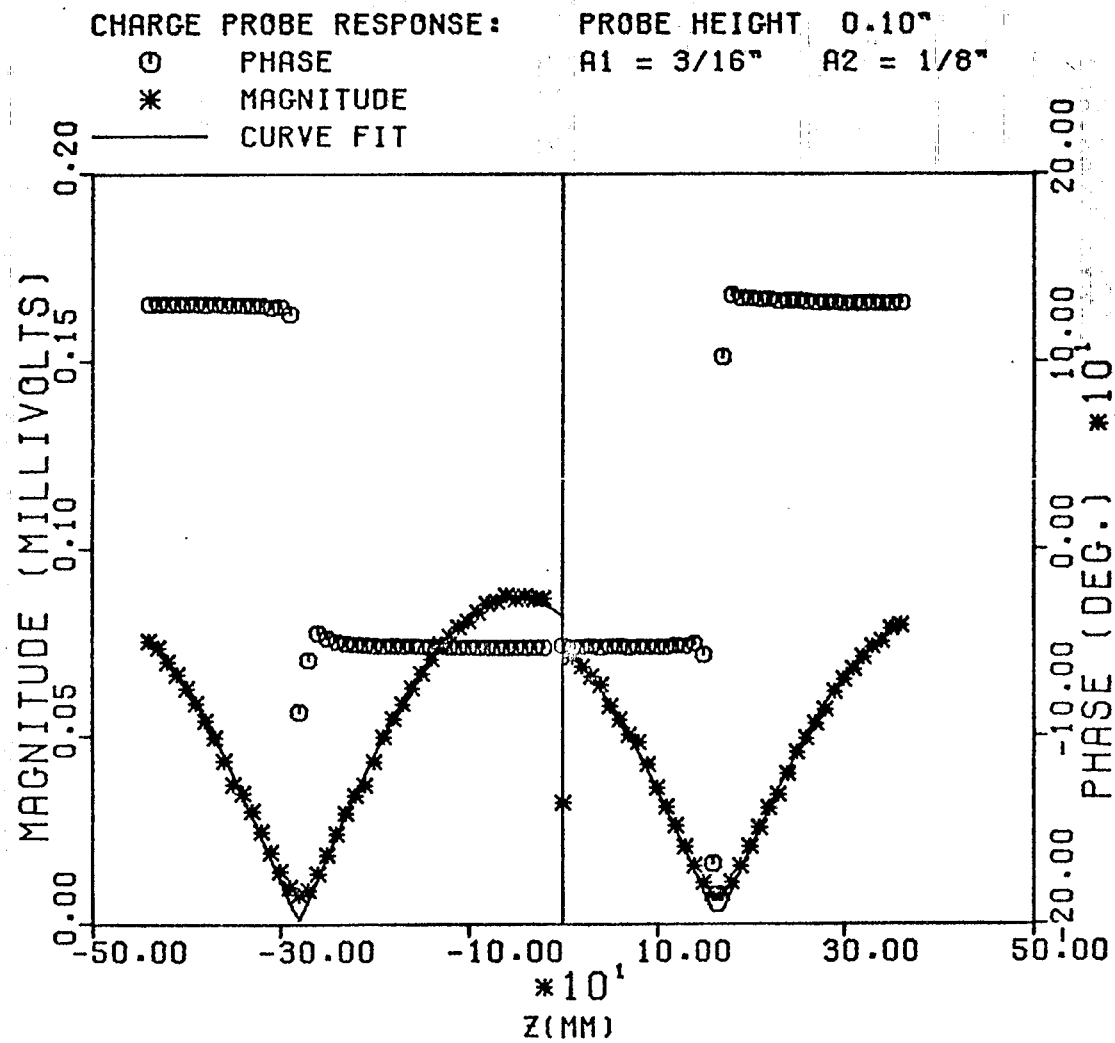
Fig. (4.11)   MEDIUM CHARGE CONDITION – PROBE HEIGHT = 0.10", a_1= 3/16"

53

CHARGE PROBE RESPONSE: PROBE HEIGHT   0.10"
  ⊙   PHASE   A1 = 3/16"   A2 = 1/8"
  ✱   MAGNITUDE
  ──   CURVE FIT
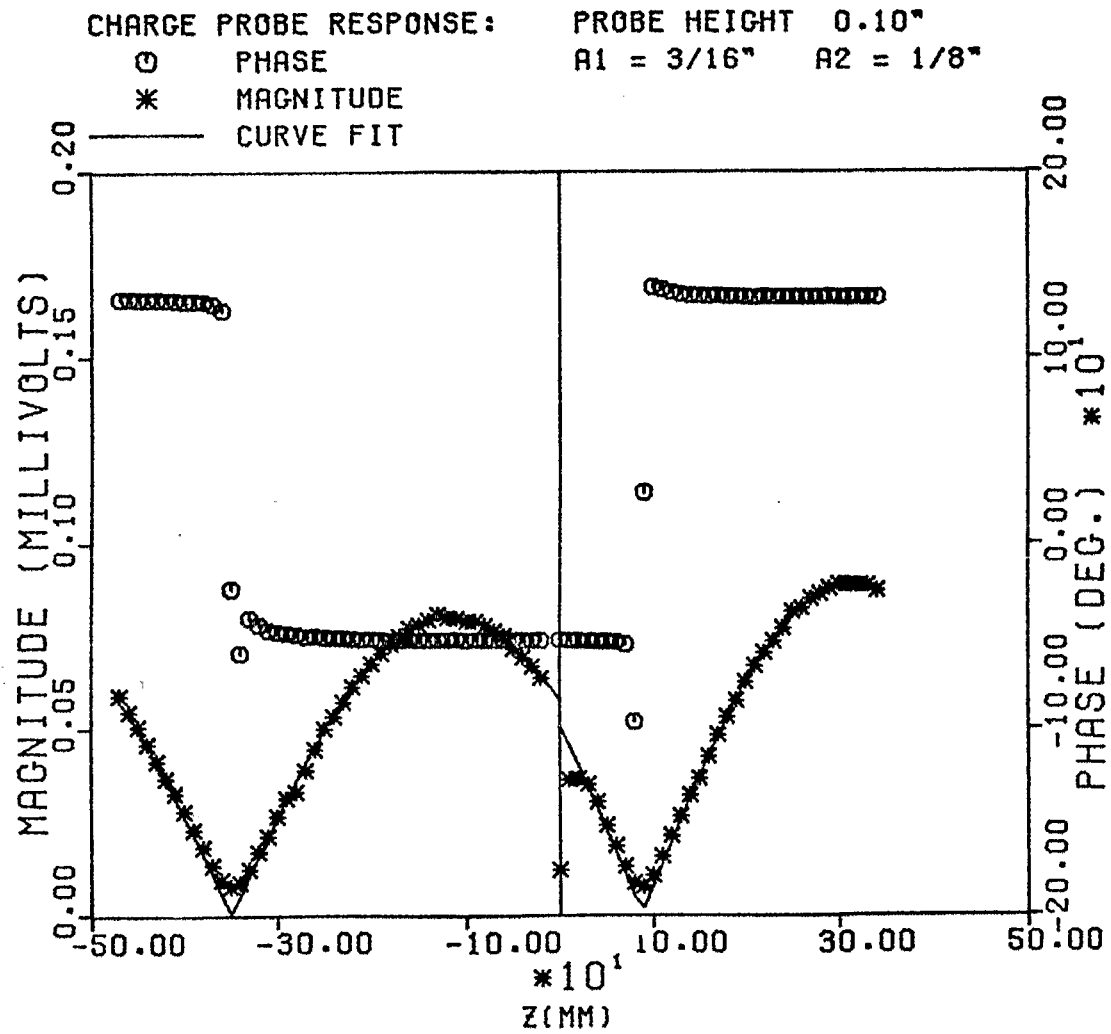
Fig. (4.12) MINIMUM CHARGE CONDITION – PROBE HEIGHT = 0.10", a_1 = 3/16"
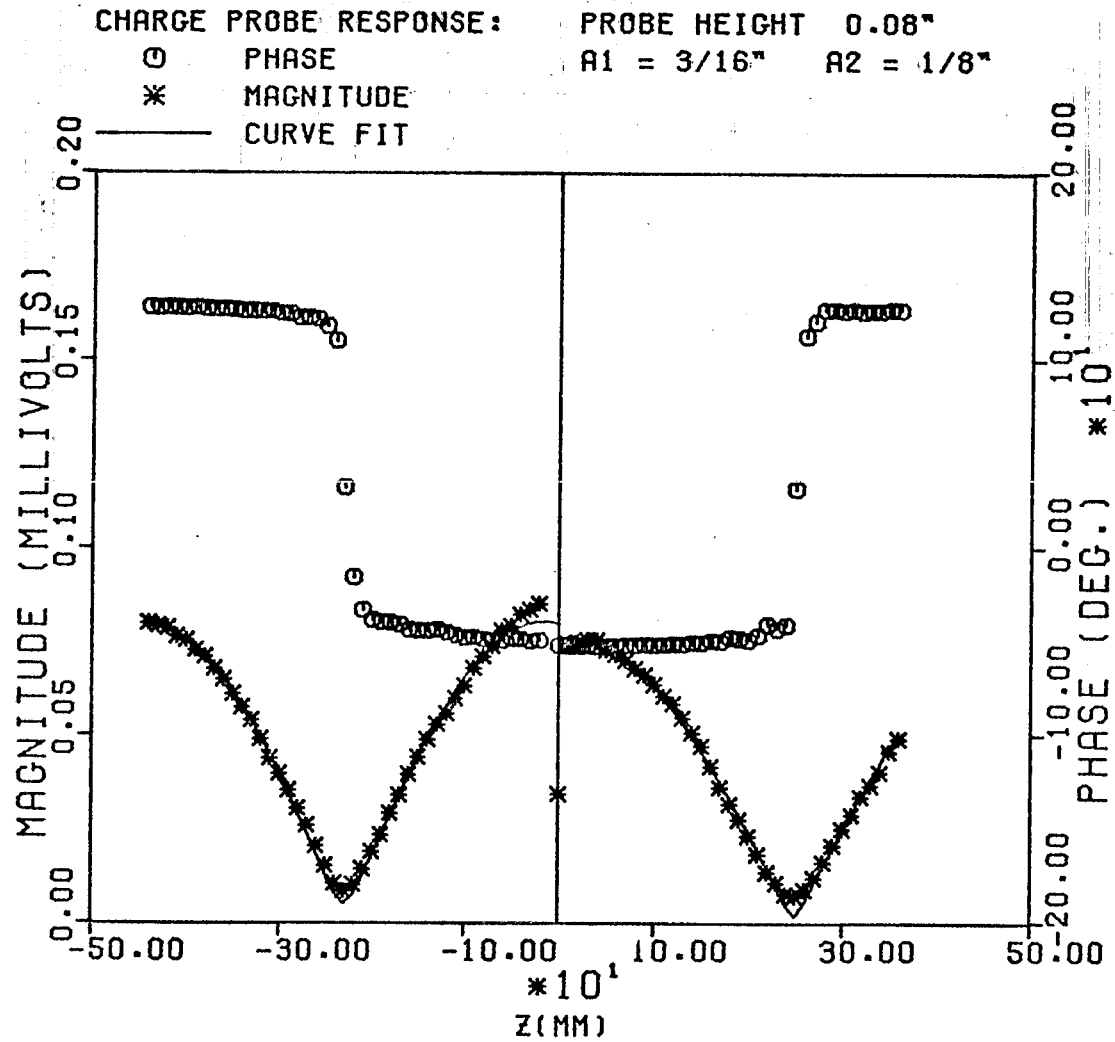
Fig. (4.13)   MAXIMUM CHARGE CONDITION - PROBE HEIGHT = 0.08", a_1 = 3/16"

CHARGE PROBE RESPONSE: PROBE HEIGHT 0.08"
  ⊙   PHASE   A1 = 3/16"   A2 = 1/8"
  ✳   MAGNITUDE
  ──   CURVE FIT
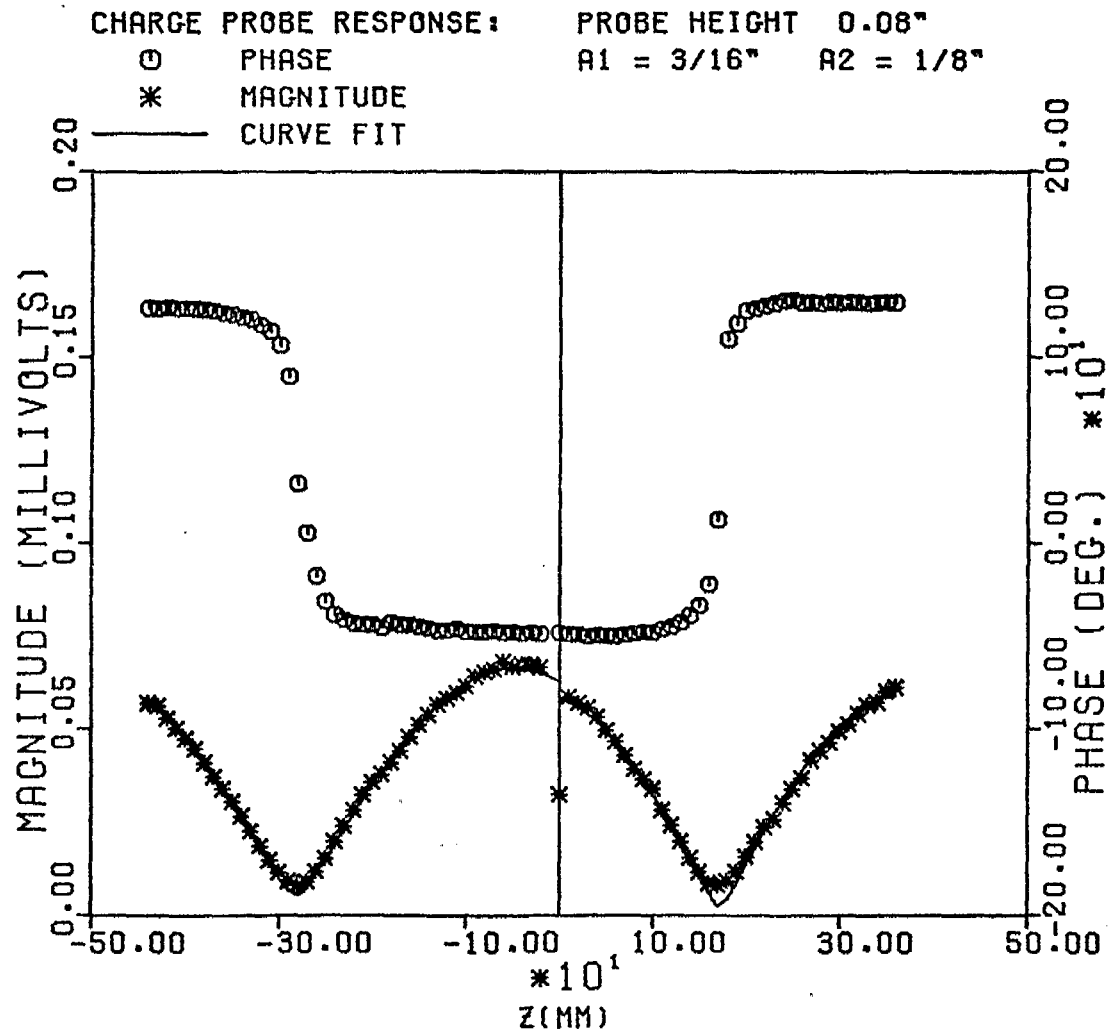
Fig. (4.14) MEDIUM CHARGE CONDITION - PROBE HEIGHT = 0.08", a_1 = 3/16"
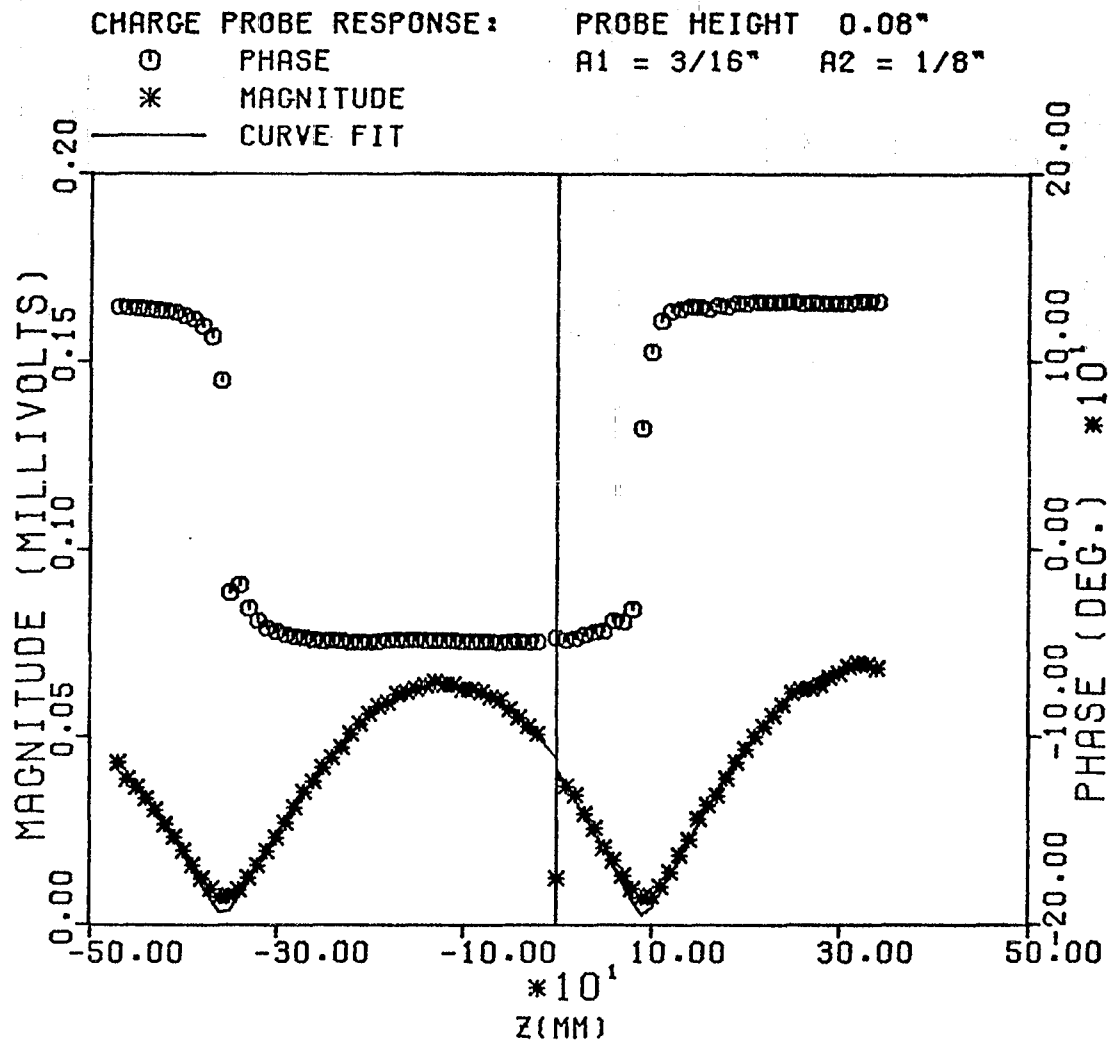
Fig. (4.15) MINIMUM CHARGE CONDITION – PROBE HEIGHT = 0.08", a_1 = 3/16"

CHARGE PROBE RESPONSE: PROBE HEIGHT   0.06"
   ☉   PHASE   A1 = 3/16"   A2 = 1/8"
   ✳   MAGNITUDE
   ——   CURVE FIT

Fig. (4.16)   MAXIMUM CHARGE CONDITION – PROBE HEIGHT = 0.06", a_1= 3/16"
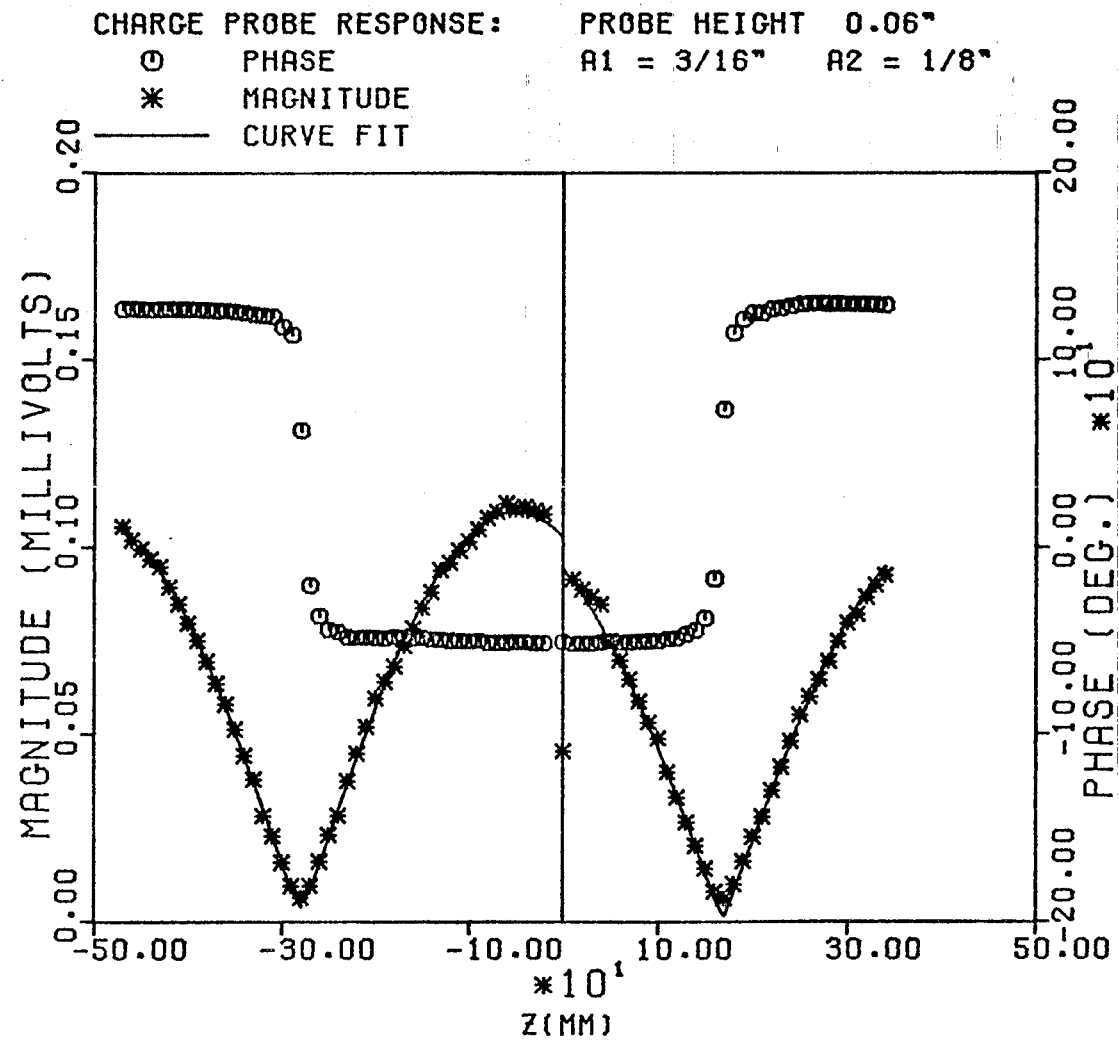
Fig. (4.17)   MEDIUM CHARGE CONDITION – PROBE HEIGHT = 0.06", a_1 = 3/16"
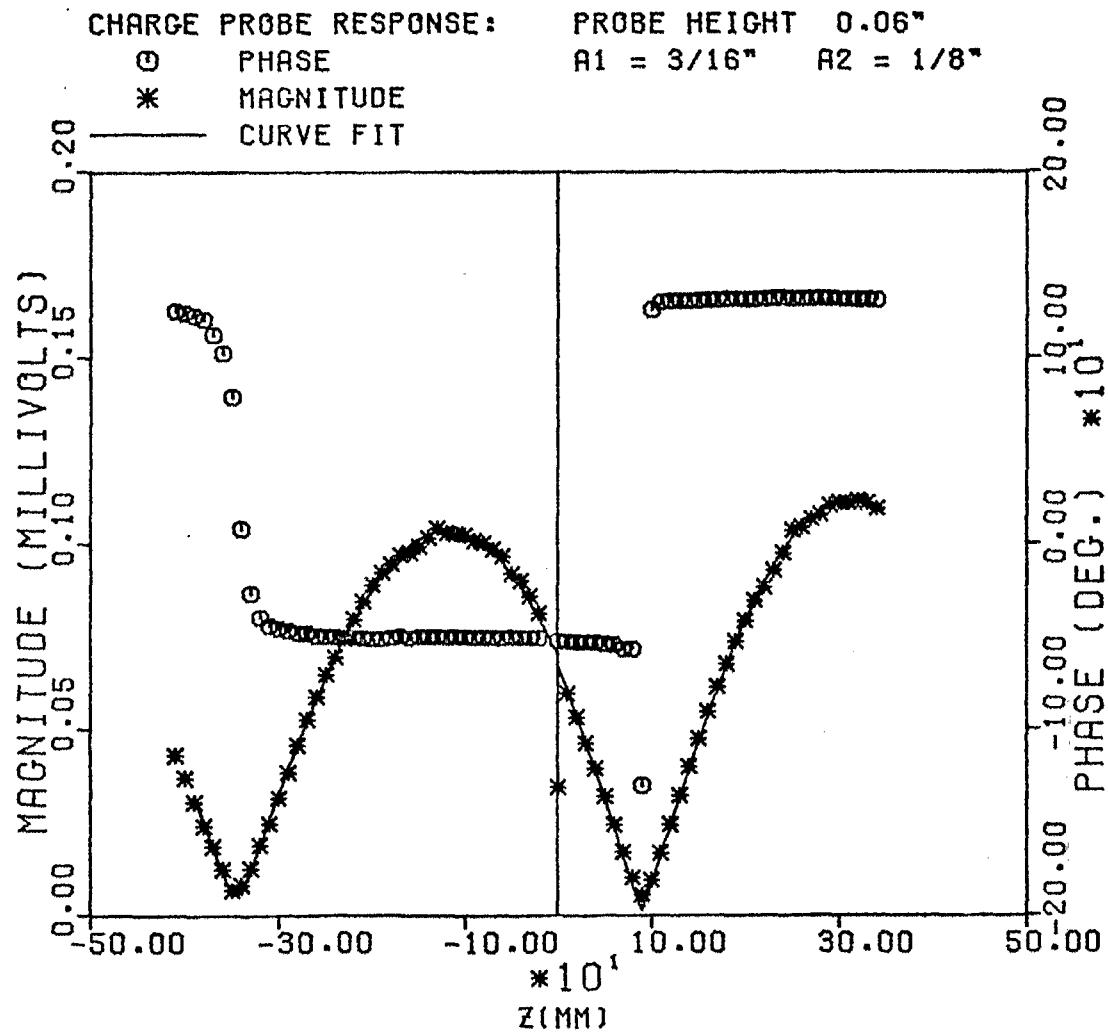
Fig. (4.18)   MINIMUM CHARGE CONDITION - PROBE HEIGHT = 0.06", a_1 = 3/16"
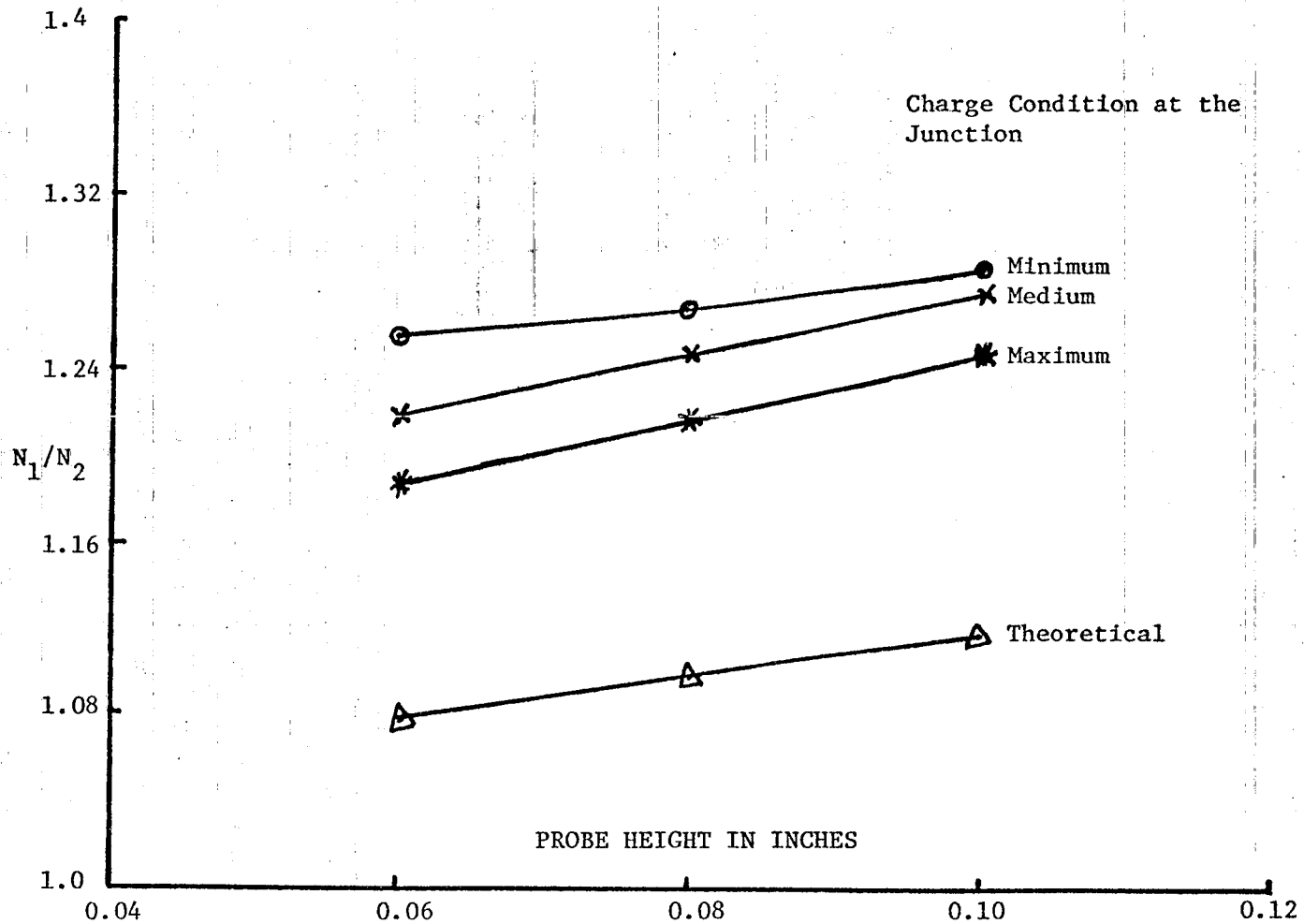
Fig (4.19)   PROBE CALIBRATION FACTOR FOR 5/16" to 1/8" RATIO OF RADII

obtained by the technique explained in Chapter III is also shown in Fig. (4.19). Similarly Fig. (4.20) presents the probe calibration factor for $a_1 = 3/16"$ and $a_2 = 1/8"$.

Examination of Figs. (4.19) and (4.20) reveals differences of about 8% in the experimental values of N_1/N_2 for different charge conditions are the junction. With the assumption that the probe responds to the local charge density at its location on the cylinder N_1/N_2 should be a function of probe height and cylinder radii only. The observed effect of the position of the junction with respect to the standing wave pattern is believed to result from inaccuracies in the extrapolation of the data to the junction. The extrapolation, and hence determination of N_1/N_2 is accomplished by fitting the curve to the measured data. Since the data is available over a distance of only $\lambda/2$ each side of the junction the accuracy in determination of the parameters for this curve is limited. For these reasons the data obtained for the case of maximum charge at the junction is the most reliable since the slope of the curve in the extrapolation region is near zero. In future use of these experimentally determined probe calibration factors greatest weight will, therefore, be given to the values determined for the maximum charge condition.

Examination of Figs. (4.19) and (4.20) also reveals a consistent difference between the measured and theoretical values of N_1/N_2. The reasons for this difference are not fully understood; however, it must be remembered that the theoretical solution is based on a planar image theory. The effects of the cylindrical geometry are the most likely
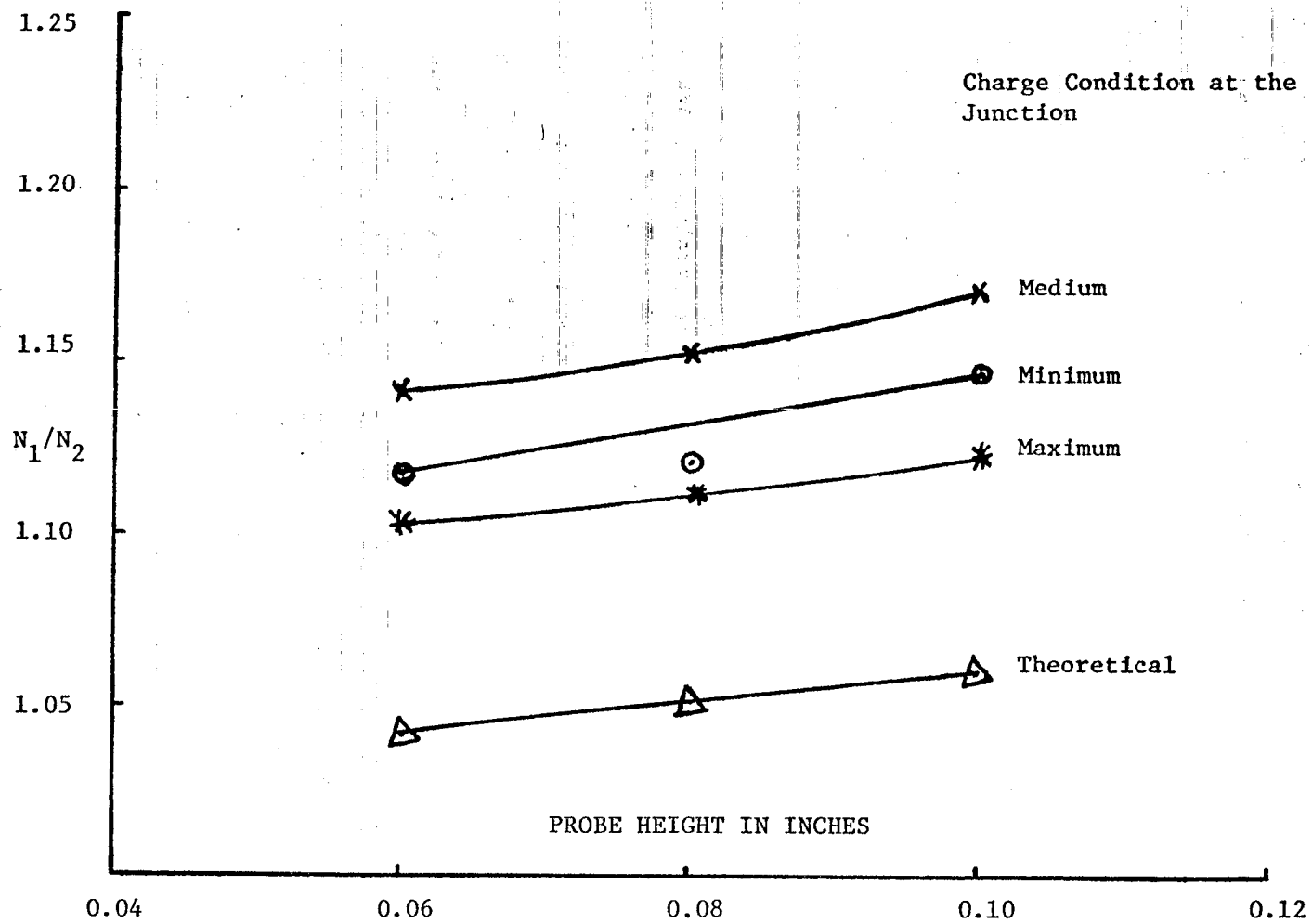
Fig. (4.20) PROBE CALIBRATION FACTOR FOR 3/16" to 1/8" RATIO OF RADII

source of the observed differences between experimental and theoretical values. Until more accurate data and theoretical solutions are available, the experimental value of N_1/N_2 will be used as the most reliable.

(iv) Conclusions

The results of this investigation have clearly demonstrated the effect of cylinder radius on the response of charge probe and have taken a considerable step toward better understanding of charge measurements. The probe calibration factors obtained can now be used to correct charge distribution measurements on structures containing junctions of unequal radii cylinders.

Further work, however, is needed for complete understanding of the response of monopole probes on nonplanar surfaces. In particular, an effort should be made to include the cylindrical image plane geometry into the theoretical treatment presented here. In addition, other probe configurations should be examined and evaluated with respect to their response on nonplanar surfaces.

REFERENCES

[1] R.W.P. King, "Quasi-Stationary and Nonstationary Currents in Electric Circuits," pp. 267-270, Encyclopedia of Physics, Edited by S. Flügge, Vol. XVI: Electric Fields and Waves, Springer-Verlag, 1958.

[2] H. Whiteside, "Electromagnetic Field Probes," Cruft Laboratory Technical Report No. 377, Harvard University, Cambridge, Massachusetts, 1962.

[3] T.T. Wu and R.W.P. King, "The Tapered Antenna and its Application to the Junction Problem for Thin Wires," IEEE Transactions on Antenna and Propagation, Vol. AP-24, pp. 42-45, January 1976, and also Interaction Note 269, January 1976.

[4] C.M. Butler, K.R. Umashankar and C.E. Smith, "Theoretical Analysis of Biconical Antenna," report submitted to the U.S. Army, STRATCOM, 1975.

[5] R.F. Harrington, Field Computation by Moment Methods, Macmillan Company, New York, 1968.

[6] N. Marcuvitz, Waveguide Handbook, McGraw-Hill Book Company, New York, 1957.

[7] Hildebrand, Introduction to Numerical Analysis, McGraw-Hill Book Company, New York, 1956.